HHS Public Access

Author manuscript

Nat Neurosci. Author manuscript; available in PMC 2019 April 22.

Published in final edited form as:

Nat Neurosci. 2018 November ; 21(11): 1530–1540. doi:10.1038/s41593-018-0249-3.

Brs3 neurons in the mouse dorsomedial hypothalamus regulate body temperature, energy expenditure and heart rate, but not food intake

Ramón A. Piñol[1,*], **Sebastian H. Zahler**[1], **Chia Li**[1], **Atreyi Saha**[1], **Brandon K. Tan**[1], **Vojtěch Škop**[1], **Oksana Gavrilova**[2], **Cuiying Xiao**[1], **Michael J. Krashes**[1], and **Marc L. Reitman**[1,*]

[1]Diabetes, Endocrinology, and Obesity Branch, National Institute of Diabetes and Digestive and Kidney Diseases, National Institutes of Health, Bethesda, MD 20892, USA

[2]Mouse Metabolism Core, National Institute of Diabetes and Digestive and Kidney Diseases, National Institutes of Health, Bethesda, MD 20892, USA

Abstract

Bombesin-like receptor 3 (BRS3) is an orphan G protein-coupled receptor that regulates energy homeostasis and heart rate. We report that acute activation of *Brs3*-expressing neurons in the dorsomedial hypothalamus (DMH^{Brs3}) increased body temperature (Tb), brown adipose tissue temperature, energy expenditure, heart rate and blood pressure, with no effect on food intake or physical activity. Conversely, activation of *Brs3* neurons in the paraventricular nucleus of the hypothalamus (PVH^{Brs3}) had no effect on Tb or energy expenditure, but suppressed food intake. Inhibition of DMH^{Brs3} neurons decreased Tb and energy expenditure, suggesting a necessary role in Tb regulation. We found that the preoptic area provides major input (excitatory and inhibitory) to DMH^{Brs3} neurons. Optogenetic stimulation of DMH^{Brs3} projections to the raphe pallidus (RPa) increased Tb. Thus, DMH^{Brs3}→RPa neurons regulate Tb, energy expenditure and heart rate, and PVH^{Brs3} neurons regulate food intake. *Brs3* expression is a useful marker for delineating energy metabolism regulatory circuitry.

*corresponding authors. ramon.pinol@nih.gov, marc.reitman@nih.gov.

Author contributions

RAP and MLR conceived and designed the study with input from MJK and OG. RAP performed and analyzed the experiments. RAP, SHZ and AS performed chemogenetic experiments, immunohistochemistry and counted cells. RAP, SHZ and BT performed optogenetic and anterograde tracing experiments. CX generated Brs3-Cre mice, performed Western blot and qRT-PCR experiments. OG performed indirect calorimetry experiments. VS and RAP performed IR experiments. CL performed electrophysiology experiments. RAP wrote the manuscript with input from MLR and all other authors.

Accession Codes

No accession codes were used for this study

Data availability. The data that support the findings of this study are available from the corresponding authors on request.

Competing Interest Statement

The authors declare no competing interests.

Introduction

Bombesin-like receptor 3 (BRS3) is an orphan G-protein coupled receptor (GPCR) that is phylogenetically well-conserved and highly expressed in specific brain regions [1,2]. BRS3 is a member of a GPCR subfamily that includes the neuromedin B and gastrin releasing peptide receptors. Mammalian BRS3 lacks a known endogenous high-affinity ligand and has a low affinity for bombesin, a frog skin peptide that is not found in mammals [3–6]. Targeted deletion of *Brs3* in mice causes obesity, mediated both by a decrease in energy expenditure and an increase in food intake, with a reduced resting body temperature (Tb) and resting heart rate [7–11]. Concordantly, BRS3 agonists increase resting Tb, energy expenditure, heart rate, blood pressure, activate brown adipose tissue (BAT) and decrease food intake [4,12–15]. The global BRS3 null phenotype is replicated by selective loss of *Brs3* in neurons expressing vesicular glutamate transporter 2 (Vglut2) [16]. Both the location of the responsible *Brs3* neuron populations and the specific circuits directing this physiology remain to be elucidated.

Brs3 is found in a limited number of brain nuclei, mostly in the hypothalamus [1,12]. *Brs3*-expressing nuclei implicated in the regulation of Tb, energy expenditure and food intake, include the dorsomedial hypothalamus (DMH), paraventricular nucleus of the hypothalamus (PVH), parabrachial nucleus (PBN) and preoptic area (POA) [1,12,17]. Thus, *Brs3* expression could be a valuable marker for elucidating the circuitry important for the treatment of metabolic diseases.

The central nervous system tightly regulates body temperature in mammals, with the purpose of maintaining homeostasis while adapting to changes in the external or internal milieu. Thermal physiology depends on the size of the organism. Large mammals are oriented towards heat loss, through environmental adaptation, vasodilation, sweating and/or panting. Small mammals focus on heat generation, including BAT activation and shivering. They also conserve heat using behavioral thermoregulation and vasoconstriction. Physiological changes to regulate Tb are initiated by sensation of the thermal environment, relayed via ascending sensory signals to the POA, which also harbors temperature-sensing neurons [18–21]. The DMH is a pivotal nucleus in the output pathway of POA neurons, receiving direct preoptic input in response to cold [22–24], or warm [18,21] ambient temperatures to regulate sympathetic activation of BAT [22,24].

Acute manipulation of defined populations of DMH neurons (eg., expressing *LepRb*, *Vglut2*, *Vgat*, *Chat*) in awake animals can alter Tb, BAT temperature, physical activity and food intake [18,21,25–27]. A thermoregulatory output pathway of the DMH is to the raphe pallidus (RPa), likely also driving cardiovascular sympathetic outflow [28–30]. This sympathoexcitatory population of DMH→RPa neurons is located in the dorsal DMH (dDMH) and extends further dorsally into dorsal hypothalamic area (DHA) [31]. *Vglut2* and *LepRb* are neuroanatomical markers for DMH→RPa neurons [22,28,31,32]. Here we elucidate the functions of *Brs3* neurons in the DMH and PVH, focusing on regulation of Tb and energy expenditure, and also examining food intake and heart rate.

Results

Brs3 expression pattern

To study the functions of cells expressing *Brs3*, *Brs3*-2A-CreER^{T2} (Brs3-Cre) mice were produced by targeted insertion of tamoxifen-inducible Cre recombinase gene into the native *Brs3* locus (Supplementary Fig. 1a). Brs3-Cre expression was visualized using a Cre-dependent tdTomato reporter line (Ai14). The concentration of tdTomato-positive neurons was highest in the POA, PVH, DMH, bed nucleus of the stria terminalis (BNST), medial posterodorsal amygdala (MePD) and lateral parabrachial nucleus (LPB) (**Supplementary Fig. 1b,c**, **Supplementary Table 1**). No tdTomato expression was observed without tamoxifen treatment. In situ hybridization demonstrated that most neurons expressing *Brs3* mRNA also express *tdTomato* mRNA and vice versa (**Supplementary Fig. 1d**). The tdTomato expression pattern is consistent with that previously reported for *Brs3* mRNA [1] and ligand binding [12]. We conclude that the Cre expression in Brs3-Cre mice faithfully reproduces the endogenous *Brs3* expression pattern.

Brs3 is located on the X chromosome and *Brs3*^{Cre} undergoes X-inactivation (see **Methods** and **Supplementary Fig. 2a**). Due to the X-inactivation, all subsequent studies used male mice.

We next investigated the phenotype of mice carrying the *Brs3*^{Cre} allele. Hypothalamic *Brs3* mRNA expression was reduced by 41 ± 3 % (**Supplementary Fig. 2b**). Brs3-Cre mice showed no difference in baseline Tb (data not shown). However, on a chow diet, the Brs3-Cre mice showed a slight but statistically significant increase in body weight, fat mass, and lean mass, compared to littermate controls; these differences were magnified by a high fat diet (**Supplementary Fig. 2c**). This phenotype suggests that the *Brs3*^{Cre} allele has reduced BRS3 function. However, the Brs3-Cre mice did respond to the selective BRS3 agonist MK-5046, by increasing Tb and reducing food intake (**Supplementary Fig. 2d-e**). Taken together, these data indicate that the *Brs3*^{Cre} allele is a hypomorph, not a null.

Activation of *Brs3* neurons by cold exposure, refeeding and leptin treatment

We examined the activation of *Brs3* neurons in response to interventions that affect energy homeostasis. Cold exposure stimulated Fos expression in *Brs3* neurons in the dDMH/DHA, medial preoptic area (MPA) and median preoptic area (MnPO), but not in the PVH, vDMH, or PBN (**Fig. 1a,b**). In contrast, refeeding after a fast increased Fos expression in *Brs3* neurons in the PVH and PBN, but not in the dDMH/DHA, vDMH, MPA or MnPO (**Fig. 1c,d**). Thus, different subsets of *Brs3* neurons are activated by cold exposure and by refeeding.

Brs3 mRNA is enriched in leptin receptor-expressing neurons [33], so we investigated if leptin activates *Brs3* neurons. Leptin treatment increased STAT3 phosphorylation in *Brs3* neurons in the MPA, MnPO, dDMH/DHA and vDMH, but not the PVH or PBN (**Supplementary Fig. 3a,b**), indicating that these neurons can be activated by leptin, likely directly.

We selected the PVH and DMH for further investigation, based on the high density of *Brs3* neurons, responses to stimuli and known role in energy balance regulation. Micro-infusion

of the selective BRS3 agonist, MK-5046, into the DMH increased BAT temperature (T_{BAT}), while drug infusion into the PVH did not (**Supplementary Fig. 3c,d**). No effect on T_{BAT} was seen with vehicle infusion into either the DMH or PVH.

Activation of DMH^{Brs3} neurons increases Tb and energy expenditure; PVH^{Brs3} neuron activation suppresses food intake

The Fos and agonist data suggest distinct functions for the DMH^{Brs3} and PVH^{Brs3} populations. To further assess their roles in energy metabolism, we used chemogenetics to selectively activate either DMH^{Brs3} or PVH^{Brs3} neurons. Viral expression and function of the excitatory designer receptor exclusively activated by designer drug (DREADD) hM3Dq (**Fig. 2a,b**) was confirmed in *ex vivo* brain slices, where the agonist clozapine-*N*-oxide (CNO) appropriately depolarized and/or increased firing of DMH^{Brs3} or PVH^{Brs3} neurons (**Supplementary Fig. 4a,b**).

In vivo, activation of DMH^{Brs3} neurons with CNO (1 mg/kg) increased light phase Tb by 1.13 ± 0.18 °C (vs 0.13 ± 0.09 °C with vehicle, p = 0.003; **Fig. 2c**). A higher CNO dose (3 mg/kg) produced a similar response, while a lower dose (0.3 mg/kg) elicited a shorter duration increase in Tb. BRS3 agonist MK-5046 increased Tb to a similar level as CNO (**Supplementary Fig. 4c**). CNO treatment of control mice lacking hM3Dq did not affect Tb or energy expenditure (data not shown). Neither MK-5046 nor CNO affected physical activity beyond the increase caused by handling and seen with vehicle treatment (**Fig. 2c,d**; **Supplementary Fig. 4d**). Chemogenetic activation of DMH^{Brs3} neurons increased energy expenditure by 33% (0.082 ± 0.017 kcal/h with CNO vs −0.003 ± 0.007 kcal/h with vehicle, p = 0.005; **Fig. 2c**). The duration of the increase in energy expenditure was shorter than the increase in Tb. Activation of DMH^{Brs3} neurons caused higher glucose levels (**Fig. 2e**, p = 0.02), but had no effect on food intake at the onset of the dark cycle following 5h of food deprivation (**Fig. 2f**). CNO did not significantly change plasma non-esterified fatty acid or glycerol levels (data not shown).

In contrast, activation of PVH^{Brs3} neurons did not alter Tb, energy expenditure, or blood glucose (**Fig. 2 d,g**). However, activation of PVH^{Brs3} neurons decreased food intake by 30.0 ± 3.6 % (**Fig. 2h**, p = 0.008). We also tested if inhibition of PVH^{Brs3} neurons could increase food intake, via viral expression of the inhibitory DREADD hM4Di (**Supplementary Fig. 4e,f**). Inhibition of PVH^{Brs3} neurons with CNO in calorically-replete mice during the light cycle increased food intake by 69 ± 16% (**Supplementary Fig. 4g**).

Taken together, these data demonstrate that activation of PVH^{Brs3} neurons does not change Tb or energy expenditure, but PVH^{Brs3} neurons can bi-directionally regulate food intake. In contrast, activation of DMH^{Brs3} neurons has no effect on food intake, but increased Tb and energy expenditure.

Adulthood ablation and acute inhibition of DMH^{Brs3} neurons reduce cold-induced thermogenesis

We next examined if ablation of the DMH^{Brs3} neurons in adulthood could affect long term body weight regulation and food intake. DMH^{Brs3} neurons were ablated by injections of a

Cre-dependent diphtheria toxin A (DTA)-expressing AAV into Brs3-Cre mice (**Supplementary Fig. 5a-c**). In the EYFP control mice, we counted 531 ± 97 (range: 267 to 862) EYFP-positive (*Brs3*) neurons in the DMH vs 44 ± 19 (range: 0 to 132) in the EYFP +DTA mice, a 92% reduction. Body weight, food intake, energy expenditure, and fat mass were not different between the groups (**Supplementary Fig. 5d-g**). No difference was seen in baseline Tb or physical activity at 22 °C (**Supplementary Fig. 5h,i**). There was a modest reduction in Tb during cold (7° C) exposure in EYFP+DTA, compared to EYFP mice (**Supplementary Fig. 5j**). There was no difference in the Tb increase produced by the stress of placing the mouse in the empty cage previously occupied by an unfamiliar male (**Supplementary Fig. 5k**). The BRS3 agonist MK-5046 increased Tb to similar levels in both groups (**Supplementary Fig. 5l**). The mild Tb phenotype of the DMH^{Brs3}-ablated mice may be due to incomplete ablation, adaptation to neuronal loss, and/or the existence of other Tb-regulating *Brs3* neurons. Thus, adulthood loss of DMH^{Brs3} neurons did not affect body weight, food intake, or energy expenditure, but modestly impaired Tb defense during cold exposure.

To determine if acute inhibition of DMH^{Brs3} neurons affects cold-induced thermogenesis, we virally expressed the inhibitory DREADD hM4Di (**Fig. 3a**). In *ex vivo* brain slices, CNO decreased the firing rate and hyperpolarized DMH^{Brs3} neurons (**Supplementary Fig. 6a**). *In vivo*, CNO reduced Tb by 1.03 ± 0.27 °C vs a 0.21 ± 0.12 °C increase with vehicle ($p = 0.02$; **Fig. 3b**). CNO also reduced energy expenditure by 17 ± 2% compared to vehicle, with no effect on physical activity. No effect of CNO was observed in wild type mice injected with the DIO-hM4Di virus in the DMH (**Supplementary Fig. 6c**). No significant reduction in Tb occurred at an ambient temperature of 34 °C (**Supplementary Fig. 6b**), at which there is no cold-induced thermogenesis to inhibit. These data suggest that under standard housing conditions (~ 22 °C) DMH^{Brs3} neurons contribute to the neural tone regulating cold-induced thermogenesis.

In addition to cold, other situations can increase Tb. We studied inhibition of DMH^{Brs3} neurons during lipopolysaccharide treatment, which causes fever via a systemic inflammatory response, and found a blunted Tb increase in CNO-treated mice (**Fig. 3c**). We next combined inhibition of DMH^{Brs3} neurons with the stress of being placed in a cage previously occupied by an unfamiliar male. The initial handling and cage switch similarly increased Tb in both groups, after which the CNO-treated mice showed a greater Tb reduction (**Fig. 3d**). These results are consistent with DMH^{Brs3} neurons being part of a common effector pathway for regulating Tb. Alternatively, they may supply a parallel signal that is integrated with other signals. This result rules out that intervention-activated circuits completely bypass or dominate over the capacity of DMH^{Brs3} neurons to regulate Tb.

Optogenetic activation of DMH^{Brs3} neurons increases Tb, heart rate, and blood pressure

Optogenetic activation of DMH^{Brs3} neurons allowed studying rapid physiological responses without handling the mice, which particularly confounds measurement of heart rate and blood pressure. We transduced DMH^{Brs3} neurons with AAV-Flex-ChR2-tdTomato (**Fig. 4a**) or control (AAV-DIO-mCherry) viruses. Stimulation of ChR2 in DMH^{Brs3} neurons increased neuronal firing in an *ex vivo* slice experiment (**Supplementary Fig. 7a**). *In vivo,*

awake mice in their home cage were studied during five cycles of 20 minutes of photostimulation, followed by [60] minutes with the laser off (**Fig. 4b**). The photostimulation triggered a rapid and robust increase in Tb with no effect on physical activity. There was no attenuation or systematic difference in Tb as a function of cycle number, so the five cycles were averaged in all further experiments. No effect was observed in mCherry-expressing control mice. Increasing stimulation frequency produced dose-dependent increases in Tb (**Supplementary Fig. 7b**).

The 20-minute stimulation duration allowed measurement of the full effect on Tb; shorter durations did not allow Tb to stabilize and longer durations did not increase it further (**Supplementary Fig. 7c**). Our standard stimulation used a 1 s on / 3 s off protocol (20 Hz, 10 ms pulses). Doubling the light dose (to 1 s on / 1 s off), doubled the initial rate of increase in Tb (**Supplementary Fig. 7c**). Thus, our standard stimulation protocol is not a maximal stimulus.

A primary effector mechanism for increasing Tb is sympathetic activation of brown adipose tissue, with other mechanisms being vasoconstriction and behavioral adaptation. To examine the effect of DMH^{Brs3} optogenetic activation on BAT thermogenesis, we used infrared imaging. At baseline, T_{BAT} was 35.7 ± 0.08 °C and lumbar temperature (T_{lumbar}) was 34.6 ± 0.09 °C. Optogenetic stimulation of DMH^{Brs3} neurons increased T_{BAT} by 1.36 ± 0.16 °C ($p = 6.8 \times 10^{-5}$) and T_{lumbar} by 1.24 ± 0.15 °C ($p = 8.9 \times 10^{-5}$) (**Fig**. **4c**, **Supplementary Fig. 7d**). T_{BAT} initially increased 1.90 ± 0.18 times faster than did T_{lumbar}. These results implicate BAT as a driver of the increase in Tb.

Sympathetic stimulation of adipose tissue causes lipolysis [34]. After optogenetic stimulation of DMH^{Brs3} neurons, we quantified phosphorylated hormone sensitive lipase (pHSL), which indicates activation of lipolysis. In BAT, but not inguinal white adipose tissue (iWAT), higher levels of pHSL were detected, demonstrating stimulation of BAT (**Supplementary Fig. 7e, 11**).

Photostimulation of DMH^{Brs3} neurons increased heart rate (HR) by 109 ± 15 bpm ($p = 0.006$), mean arterial blood pressure (MAP) by 10.2 ± 3.4 mmHg ($p = 0.047$) and Tb by 0.48 ± 0.09 °C ($p = 0.007$), without an effect on physical activity (**Fig. 4d**). The increase in heart rate and MAP was rapid, with HR reaching near-maximum levels in under 30s (**Supplementary Fig. 7f)**. In contrast, the change in Tb was slower, due to the heat capacity of the body. Photostimulation during the dark phase produced similar increases in heart rate, MAP and Tb (**Supplementary Fig. 8a**). Doubling the laser duty cycles (from 1s on, 3s off to 1s on, 1s off) produced greater increases in HR (185 ± 35 bpm) and MAP (17.3 ± 3.2 mmHg) (**Supplementary Fig. 8b**).

$DMH^{non\text{-}Brs3}$ neurons increase Tb and physical activity

Next, we probed the possibility that additional DMH neurons besides DMH^{Brs3} neurons regulate Tb. We selectively expressed ChR2 in $DMH^{non\text{-}Brs3}$ neurons using a ‘Cre off’ virus in Brs3-Cre mice. These mice will express ChR2 in all DMH neurons except those expressing Cre (**Supplementary Fig. 9a**). We also expressed this virus in wild type mice, lacking Cre, in which all infected DMH neurons (both DMH^{Brs3} and $DMH^{non\text{-}Brs3}$) express

ChR2 (DMH::ChR2). Upon optogenetic stimulation, DMH::ChR2 mice increased their Tb by 1.80 ± 0.17 °C (p = 0.002) and physical activity by 74 ± 15 counts (p = 0.02; **Supplementary Fig. 9b**). DMH$^{non\text{-}Brs3}$::ChR2 mice increased their Tb by 1.08 ± 0.15 °C (p = 0.0002) and physical activity by 75 ± 17 counts (p = 0.005). The massive activity increases contrast with the lack of activity increase upon stimulation of DMH^{Brs3} neurons and likely accounts for at least some of the Tb increase in the DMH$^{non\text{-}Brs3}$::ChR2 mice (**Fig. 4b,e** and **Supplementary Fig. 9b**). Optogenetic activation of DMH$^{non\text{-}Brs3}$ neurons did not warm up T_{BAT} significantly faster than T_{lumbar} (**Supplementary Fig. 9c,d**).

DMH^{Brs3}→RPa pathway increases Tb and receives input from POA and other nuclei

We anterogradely traced the projections of DMH^{Brs3} neurons using AAV-DIO-synaptophysin-mCherry. Major projections were to the RPa, PVH and various POA nuclei (**Supplementary Fig. 10**). The DMH^{Brs3} neurons also projected to the ventrolateral periaqueductal grey (vlPAG), nucleus accumbens, LH, locus coeruleus, and caudal, but not rostral, ventrolateral medulla. Other less densely innervated brain regions included BNST, paraventricular nucleus of the thalamus (PVT) and arcuate nucleus (Arc).

DMH projections to the RPa can stimulate BAT and increase Tb in anesthetized rats [28,29,35]. We tested the ability of the DMH^{Brs3}→RPa projections to increase Tb, by infecting DMH cell bodies with AAV-Flex-ChR2 and photostimulating the RPa. Stimulating the DMH^{Brs3}→RPa terminals increased Tb by 0.43 ± 0.12 °C (p = 0.006), with no effect on physical activity and no effect on Tb or activity in mCherry controls (**Fig. 5a-c**). Thus, selective activation of the DMH^{Brs3}→RPa pathway is sufficient to increase Tb, most likely through glutamatergic projections [1,16,28,29,32]. Indeed, DMH^{Brs3}→RPa neurons rarely expressed Gad2 (2.6 ± 0.5%), a marker for GABAergic neurons (**Fig. 5d**). Thus, we hypothesize that the DMH^{Brs3}→RPa neurons are glutamatergic.

To identify the neuronal inputs to the DMH^{Brs3}→RPa pathway, we used projection-specific rabies monosynaptic retrograde tracing. DMH^{Brs3}→RPa neurons were mostly located in the dDMH/DHA and not the vDMH (**Fig. 6a,b**). We found 28 ± 13 DMH^{Brs3}→RPa starter neurons and 304 ± 142 input neurons projecting to the starter neurons. Areas with the highest concentration of input neurons were the MPA, Arc and portions of the DMH (vDMH and posterior DMH). Notably, most of the Arc input neurons were located in the posterior Arc (ArcP; caudal to Br −2.06). Brain regions with intermediate to high density levels of input were the parabrachial nucleus (mostly LPB) and raphe interpositus nucleus and raphe magnus (RIP/RMg). Areas with intermediate input numbers included several preoptic and other hypothalamic nuclei, as well as the zona incerta and vlPAG (**Fig. 6c-i**). Sparse input areas include the cortex (anterior portion of cingulate cortex), nucleus accumbens (shell and core), medial and lateral septum, ventral pallidum, lBNST and central nucleus of the amygdala. Other areas with sparse input neurons were the suprachiasmatic nucleus, subfornical organ, PVT, medial tuberal region, lateral habenula and ventral premammillary nucleus. In the medulla, sparse GFP neurons were found in the nucleus of the solitary tract and the rostral ventrolateral medulla. No GFP neurons were found at the injection site when only EnvA-G-deleted-Rabies-GFP was injected in the RPa (without RG or TVA viruses). We

did not observe any collaterals of DMH^{Brs3}→RPa neurons in other DMH^{Brs3} projection areas, suggesting that the DMH^{Brs3}→RPa neurons project only to the RPa.

Most Tb regulation models implicate GABAergic projections from various POA regions to DMH to control Tb [18,21,22]. To evaluate the neurotransmitter input from the preoptic area to DMH^{Brs3}→RPa neurons we performed ChR2-assisted circuit mapping (CRACM). We transduced POA neurons with AAV-ChR2-EYFP and enabled identification of DMH^{Brs3}→RPa neurons with HSV-lsl-mCherry injected in the RPa. We found that the majority of DMH^{Brs3}→RPa neurons recorded receive both GABAergic and glutamatergic input from the POA (**Fig. 7**). This indicates that the DMH^{Brs3}→RPa circuit is under dynamic control by the POA.

Discussion

Genetic and pharmacologic experiments have demonstrated a role for BRS3 in the control of Tb, energy expenditure, food intake and heart rate. We investigated the responsible neurons, showing that DMH^{Brs3} neurons regulate Tb, energy expenditure and heart rate, while not affecting food intake or physical activity. More specifically, DMH^{Brs3} neurons use a DMH^{Brs3}→RPa pathway to bidirectionally control Tb, including via action on brown adipose tissue. In contrast, PVH^{Brs3} neurons control food intake and do not affect Tb, energy expenditure, or physical activity. These results suggest a mechanistic basis for the phenotype of *Brs3* knockout mice. Loss of BRS3 from the DMH^{Brs3} neurons could contribute to the reduced resting Tb, energy expenditure and heart rate. Loss of BRS3 from PVH^{Brs3} neurons could promote the increased food intake. Together, these mechanisms contribute to the obese phenotype of the global null mice.

The simplicity of this model notwithstanding, a caveat is that genetic *Brs3* ablation nullifies only the contribution of one receptor (and its elusive ligand), while optogenetic and chemogenetic manipulations probe the properties of the neuron expressing this receptor. The current study does not address whether BRS3 in neurons in other areas also contribute, possibly redundantly, to the regulation of Tb, energy expenditure, heart rate and food intake. For example, we observed that PBN^{Brs3} neurons are activated during refeeding, which could indicate a role in regulating food intake or signaling nutritional status. Similarly, the activation of MPA^{Brs3} and $MnPO^{Brs3}$ neurons by a cold environment suggests the possibility of contribution to the regulation of thermogenesis by these populations. Recently, *Brs3* mRNA was found to be enriched in a warm-sensitive population of POA (predominantly Gad2/BDNF/PACAP-expressing) neurons [18]. Paradoxically, we observed very low Fos expression in MPA^{Brs3} and $MnPO^{Brs3}$ neurons after warm exposure. Possibly, *Brs3* neurons in different preoptic nuclei provide complementary contributions to Tb regulation. This discrepancy could also be due to the different warm conditions (30 °C vs 37 °C).

The Brs3-Cre allele is hypomorphic, as are others in widely used knock-in Cre lines (e.g., somatostatin-IRES-Cre [36], DTA-Cre, https://www.jax.org/strain/006660). Our observations about DMH^{Brs3} and PVH^{Brs3} neurons are likely not compromised by the Brs3-Cre's hypomorphism since the mice do respond to BRS3 agonist. Additionally, we used *Brs3* as a

neuronal marker, focusing on the circuitry and function of *Brs3* neurons, and not the function of the BRS3 receptor per se.

Multiple lines of evidence suggest that the DMH→RPa pathway that activates BAT is glutamatergic. Glutamate receptor antagonist administration in the RPa inhibits increased BAT sympathetic nerve activity and temperature, evoked by pharmacological disinhibition [29] or optogenetic [28] stimulation of the DMH. *Brs3* and Vglut2 colocalize in the DMH by in situ hybridization [1]. Also, germline deletion of *Brs3* in glutamatergic, but not GABAergic, neurons recapitulates the Tb phenotype of the global *Brs3* knockout and re-expression of *Brs3* in glutamatergic, but not GABAergic, neurons reversed the null phenotype [16]. Indeed, we found that DMH^{Brs3}→RPa projecting neurons rarely express Gad2.

The PVH contains multiple neuronal types that regulate food intake, including those expressing *MC4R* [37], *BDNF* [38], *AVP* [39] and non-Oxt *Nos1* [40]. The PVH^{Brs3} neurons could be a subpopulation of any of these, except the appetite-regulating BDNF neurons, which appear to be located more rostrally [38]. The downstream circuits through which the PVH^{Brs3} neurons exert their functions are not known. Since re-expression of BRS3 in Vglut2-positive neurons normalizes the increased food intake of *Brs3* null mice and is sufficient for suppression of food intake by BRS3 agonist [16], the relevant PVH^{Brs3} neurons are probably glutamatergic.

The predominant mechanism of cold-induced thermogenesis in mice is sympathetic activation of BAT, causing heat production via substrate oxidation uncoupled from ATP generation [22,41]. We demonstrated that DMH^{Brs3} neurons increase BAT temperature, preceding the Tb increase, suggesting that BAT is driving the Tb increase. A subpopulation of DMH neurons contributes to the sympathetic regulation of both BAT and WAT [42]. DMH^{Brs3} stimulation caused BAT activation, also demonstrated by increased phosphorylation of HSL. DMH^{Brs3} neuronal activation did not produce a detectable increase in plasma non-esterified fatty acid or glycerol levels. It is possible that longer duration of stimulation [34] would demonstrate WAT activation. We have not investigated if activation of DMH^{Brs3} neurons also modulates other thermoregulatory mechanisms, such as vasodilation/vasoconstriction, shivering, or behavioral adaptation [23].

Brs3 knockout mice have a reduced resting heart rate, which increases disproportionally with physical activity, reaching a similar upper limit as in wild type mice. Blood pressure in *Brs3* knockout and wild type mice is similar at rest, but increases more with activity and stress in the *Brs3* knockout mice [7,10]. A working model is that *Brs3* knockout mice have a reduced resting sympathetic tone and heart rate, which increase disproportionally with activity. The resting blood pressure is defended by feedback regulation and overshoots during physical activity. BRS3 agonists acutely increase heart rate and blood pressure, effects that attenuate with continued treatment over hours to days [10,13,14]. Optogenetics allows study of acute cardiovascular parameters without handling perturbations. Optogenetic activation increased heart rate and arterial pressure, demonstrating that DMH^{Brs3} neurons are sufficient to produce these effects. This result suggests that, from a therapeutic standpoint, it will be difficult to dissociate the desired activation of BAT by BRS3 agonists from the undesired increases in heart rate and blood pressure. The obesity-associated

increase in mouse blood pressure may implicate leptin signaling, possibly through leptin receptors in the DMH [43]. DMH^{Brs3} neurons, a large fraction of which are activated by leptin, might overlap with the DMH^{LepRb} neurons involved in blood pressure increases in obesity.

DMH^{Brs3} neurons contribute to cold-induced thermogenesis and their activation increased Tb and energy expenditure, without altering physical activity. In contrast, activation of $DMH^{non\text{-}Brs3}$ neurons greatly increased activity, which likely accounts for at least some of the concomitant increase in Tb. Other studies of the DMH have identified DMH^{LepRb}, DMH^{Vglut2} and DMH^{Vgat} neurons as increasing physical activity, Tb, and energy expenditure [21,26]. These observations suggest that *Brs3* is a marker for a distinct subpopulation, regulating the sympathetic nervous system independent of physical activity.

The heart rate increase from DMH^{Brs3} neuron activation may be important for increasing blood flow to activated BAT, bringing fuel (glucose, fatty acids) and distributing heat to the rest of the body. It is also plausible that heat from the increased cardiac work contributes to increasing Tb.

Nakamura and colleagues investigated projections of DMH neurons and found that only the DMH neurons projecting to the RPa (and not the PVH or vlPAG) activated BAT [28]. DMH^{LepRb} neurons also project to RPa [31]. We found that some $dDMH/DHA^{Brs3}$ neurons are activated by leptin, although we did not determine the overlap with $DMH^{Brs3}\rightarrow$RPa neurons. The $DMH^{Brs3}\rightarrow$RPa projections are sufficient to increase Tb and these neurons do not appear to have collaterals. However, it remains possible that DMH^{Brs3} pathways in addition to $DMH^{Brs3}\rightarrow$RPa increase Tb.

Multiple areas of the brain project to the DMH [44] and we found that many provide input to $DMH^{Brs3}\rightarrow$RPa neurons. Suprahypothalamic input to the DMH possibly mediates autonomic responses to stress [35,45,46]. However, we did not observe substantial cortical input to $DMH^{Brs3}\rightarrow$RPa neurons, suggesting that they are not central to this response. We found that RIP/RMg neurons project to $DMH^{Brs3}\rightarrow$RPa neurons; the RIP/RMg to DMH input was not previously reported[44]. In confirmation, we have also observed labeled RIP/RMg neurons with Rabies-GFP injected in the DMH (unpublished observations, Ramón Piñol). An interesting function for LPB input to $DMH^{Brs3}\rightarrow$RPa neurons could be to relay ascending thermosensory information directly to the DMH, independent of the LPB to POA pathway [47]. Finally, significant numbers of labeled neurons in the vDMH and posterior DMH suggest intra-DMH circuitry.

$DMH^{Brs3}\rightarrow$RPa neurons receive abundant synaptic input from preoptic nuclei. DMH-regulated BAT thermogenesis is under inhibitory preoptic control [18,23,30,48,49], and possibly excitatory as well [50]. Our data suggest that $DMH^{Brs3}\rightarrow$RPa neurons are regulated by both GABAergic and glutamatergic preoptic neurons. Further research is needed to determine which POA neurons provide the inhibitory and excitatory inputs to $DMH^{Brs3}\rightarrow$RPa neurons.

In summary, we identify two *Brs3* populations with separate functions. PVH^{Brs3} neurons can robustly regulate food intake without affecting Tb. DMH^{Brs3} neurons regulate Tb, energy expenditure, BAT activity, heart rate and blood pressure, with no effect on food intake or physical activity. The data demonstrate the existence of a $DMH^{Brs3}\rightarrow$RPa population

dedicated to thermogenesis. *Brs3* is a neuronal marker useful for dissecting the neural circuits controlling energy homeostasis.

Materials and Methods

Animals.

Animal studies were approved by the NIDDK/NIH Animal Care and Use Committee. Mice were singly housed at 22 C with lights on 6 am-6 pm and fed chow (7022 NIH-07 diet, 15% kcal fat, energy density 3.1 kcal/g, Envigo Inc., Indianapolis, IN). Food and water were available ad libitum, including during drug treatments, indirect calorimetry and optogenetic experiments. Mice: Brs3-Cre (see below), B6.Cg-Gt.(Rosa)26Sortm6(CAG-ZsGreen1)Hze/J, with Cre-dependent ZsGreen (Ai6; Jax# 007906) [51], B6.Cg-Gt(ROSA)26Sortm14(CAG-tdTomato)Hze/J, with Cre-dependent tdTomato (Ai14; Jax# 007914) [51], Gad2–2a-NLS-mCherry (Gad2-mCherry; Jax# 023140)[52]. Male mice were used, unless otherwise noted. For all behavioral and physiological studies, male mice were between 8 and 45 weeks of age. Mice for electrophysiological studies to test DREADD and ChR2 function (male and female) and for CRACM studies (male) were between 5 and 13 weeks of age. Mice were on a mixed C57BL/6J and 129SvEv background. Mice from multiple litters were used for all studies.

Brs3–2A-CreERT2 mice.

Generation.—A targeting vector using C57BL/6 targeting arms and DTA negative selection was designed to insert a 2A peptide, CreERT2 recombinase, thymidine kinase polyA signal and Frt-flanked neo selection cassette, replacing the TAG stop codon in the third exon of the Brs3 gene (Cyagen, Sunnyvale, CA). The 2A sequence adds EGRGSLLTCGDVEENPG to the C-terminus of BRS3 and a proline to the N-terminus of CreERT2; it is expected that the two proteins are translated in a 1:1 ratio [53]. This construct was electroporated into TC1 ES cells (129SvEv) and correctly targeted cells were injected into Black Swiss blastocysts (Mouse Knockout Core, NIDDK). Chimeric mice were bred with FLPo10 mice (#011065, Jackson Laboratory) to delete the neo cassette and then to C57BL/6J mice to remove the FLPo10 transgene to obtain Brs3–2A-CreERT2 (Brs3-Cre) mice.

Tamoxifen.—Cre-mediated recombination was achieved by treatment with tamoxifen (110 mg/kg ip in corn oil, unless otherwise noted; Sigma Aldrich) daily for 5 consecutive days, with mice studied ?2 weeks after the last dose. Lower tamoxifen doses produced fewer tdTomato-positive neurons in Brs3Cre/+;Ai14/+ mice and higher doses were occasionally lethal.

Brs3-Cre mice validation.

Fluorescent in situ hybridization.—Mice were anesthetized (chloral hydrate, 500 mg/kg ip). Next, brains were removed, frozen on dry ice, embedded in M1 Embedding Matrix (Thermoscientific Fisher, Waltham, MA), cut on a cryostat (Leica CM 1860), adhered to SuperFrost Plus slides (VWR) and immediately refrozen. Samples were fixed in fresh 10% neutral buffered formalin solution (Sigma Aldrich), processed according to

RNAscope fluorescent Multiplex Assay manual (Advanced Cell Diagnostics; probe 454111 for Brs3 and 317041-C2 for tdTomato) and cover slipped with HardSet antifade mounting medium with DAPI.

BRS3 function.—To quantify Brs3 mRNA levels, hypothalamic tissue RNA was extracted (Qiagen Allprep DNA/RNA micro Kit, Germantown, MD). RNA was reverse transcribed (Roche Transcriptor High Fidelity cDNA Synthesis Kit, Indianapolis, IN). cDNA was quantified by real-time polymerase chain reaction (q-PCR, Applied Biosystems QuantStudio Real-Time PCR System, Foster City, CA) using SYBR green, normalized to 18S RNA.

To test the possibility of hypomorphism in Brs3-Cre mice, 6-week-old Brs3Cre/Y and Brs3+/Y littermates were singly housed and monitored for body weight, body composition (EchoMRI, EMR-122, Echo Medical Systems) and food intake. Mice were fed high-fat diet (60% kcal fat, 5.24 metabolizable kcal/g; D12492, Research Diets) at 8 weeks. Energy expenditure was estimated by energy balance [54]. To test functionality of BRS3 in Brs3-Cre mice, Tb and food intake response to BRS3 agonist MK-5046 [55] (generous gift from Merck; 10 mg/kg in saline) was tested.

X-inactivation.—Brs3 is located on the X chromosome, so the Brs3Cre allele could undergo X-inactivation [56]. Neurons expressing tdTomato were counted in heterozygous (Brs3Cre/+;Ai14/+) and homozygous (Brs3Cre/Cre;Ai14/+) female mice, carrying one vs two copies, respectively, of the Brs3Cre allele. In the three regions studied (PVH, BNST and MePD) the heterozygous females had half the number of tdTomato-positive neurons as the homozygous females (**Supplementary Fig. 2a**). The number of tdTomato-expressing neurons was similar in hemizygous male (Brs3Cre/Y;Ai14/+) and homozygous female mice.

Experimental paradigms to probe neuronal activity.

Warm/Cold Exposure.—Mice were habituated for 2–3 days at 22 C in a temperature-controlled chamber in their home cages. For the warm- (cold-) exposed group, chow was removed and the chamber was set to 30 C (4 C) at 8:30 AM. Cage interior temperature was continuously monitored using a temperature logger (HOBO data logger) and reached the target temperature in 60 minutes. After 4 hours in the chamber, the mice were perfused, their brains processed for immunohistochemistry and neurons scored for Brs3 (tdTomato) and Fos expression.

Fast/refeed.

Mice began fasting in their home cages at 3:00 PM. After 20 hours, they were either perfused immediately or given access to chow for 2 hours and then perfused and scored for Brs3 (tdTomato) and Fos expression.

Leptin treatment.

Mice began fasting in their home cages at 3:00 PM. After 20 hours, they were injected with either saline or leptin (4 mg/kg ip). After 1 hour, mice were perfused and neurons scored for Brs3 (tdTomato) and pStat3 expression.

Immunohistochemistry.

Tissue Preparation.—Mice were anesthetized (chloral hydrate, 500 mg/kg ip), perfused transcardially with 0.9% saline followed by 10% neutral buffered formalin, and the brain was removed. Brains were post-fixed (10% formalin, room temperature, 4 hours) and incubated in 20% sucrose in 0.1M PBS (4?C, overnight), sectioned coronally into three equal series (50 ?m sections) on a sliding microtome (SM2010 R, Leica) and collected in 0.1M PBS. Sections were washed 3×10 minutes in 0.1M PBS and the following steps were performed with shaking at room temperature and in 0.1M PBS solutions, unless noted otherwise:

Fos.—Sections were blocked for 2 hours in 0.5% Triton X-100, 2% normal horse serum (NHS) and then incubated (48 hours, 4?C) with 1:2000 rabbit-anti-phospho-cFos (Ser32; #5348, Cell Signaling Technology)[57] in 0.5% Triton X-100, 2% NHS. Sections were washed, incubated (4 hours) with secondary antibody (1:1000 488-donkey-anti-rabbit secondary, Abcam, Cambridge, MA, in 0.5% Triton X-100, 2% NHS) and washed, mounted and cover slipped with hardset antifade mounting medium containing DAPI (Vectashield).

pSTAT3.—Sections were incubated for 20 minutes in 1% NaOH and 0.3% H2O2, 10 minutes in 0.3% glycine in 0.1M PBS, 10 minutes in 0.03% SDS and blocked for 1 hour in 3% normal donkey serum (NDS), 0.3% TritonX-100. Sections were then incubated overnight in 3% NDS, 1:250 rabbit anti pSTAT3 (Tyr705; #9131S, Cell Signaling Technology)[58], 1:250 goat anti DsRed (L-18) (sc-33353, Santa Cruz)[59] and 0.3% Triton X-100 diluted and washed 6×8 minutes. Next, sections were incubated 1 hour with secondary antibodies (1:250 488-donkey-anti-rabbit, 1:250 594-donkey-anti-goat (both Abcam), 3% NDS and 0.3% Triton X-100). Sections were then rinsed, mounted and cover slipped with hardset antifade mounting medium containing DAPI.

mCherry.—Sections were incubated for 1 hour in 0.3% Triton X-100, 3% normal donkey serum (NDS) and then incubated overnight with 1:2000 rabbit-anti-DsRed (ab 632496, Clontech)60 in 0.3% Triton X-100, 3% NDS. Sections were washed, incubated (2 hours) with secondary antibody (1:500 Alexa-594 donkey-anti-rabbit; Invitrogen) in 0.5% Triton X-100 and 2% NHS and washed, mounted and cover slipped with hardset antifade mounting medium containing DAPI (Vectashield).

Stereotaxic injections.

General surgical procedures.—Mice were anesthetized with 0.5–1.5% isoflurane (1 L per minute of oxygen) or a ketamine/xylazine mix (80/10 mg/kg) and placed in a stereotaxic instrument (Digital Just for Mouse Stereotaxic Instrument, Stoelting). Ophthalmic ointment (Puralube, Dechra) was applied. All injections were done with pulled-glass pipettes (pulled 20–40 m tip diameter; 0.275 ID, 1 mm OD, Wilmad Lab Glass) at a visually controlled rate of 50 nl per min with an air pressure system regulator (Grass Technologies, Model S48 Stimulator). The pipette was kept in place for 5 min after injection. Post-surgery mice received subcutaneous sterile saline injections to prevent dehydration and analgesic (buprenorphine; 0.1 mg/kg).

Viral vectors.—We used the following viruses AAV8-hSyn-DIO-hM3Dq-mCherry, AAV8-hSyn-DIO-hM4Di-mCherry, AAV8-Ef1a-FLEX-TVA-mCherry, AAV8-Eff1a-DIO-mCherry and AAV8-ef1a-mCherry-FLEX-DTA (University of North Carolina Vector Core)[61]; AAV8-hSyn-DIO-hM3Dq-mCherry and AAV8-hSyn-DIO-hM4Di-mCherry (Addgene); AAV2-ef1a-DIO-GFP, AAV9-Ef1a-ChR2-Eyfp, AAV9-CAG-FLEX-ChR2-tdTomato (gift from Scott Sternson, Addgene plasmid #18917; University of Pennsylvania Viral Vector Core); AAV8-Ef1a-DIO-synaptophysin-mCherry (Virovek, Inc), AAV8-CAG-FLEX-RabiesG(Y733F) (Stanford University Vector Core); HSV-Ef1a-lsl-mCherry and HSV-Ef1a-lsl-Eyfp (Massachusetts Institute of Technology, Viral Core Facility); EnvA-G-Deleted-Rabies-Egfp (Gene Transfer, Targeting and Therapeutics Core at Salk Institute); AAV9-Ef1a-DO-hChR2(H134R)-mCherry (gift from Bernardo Sabatini; Addgene plasmid 37082; Vigene Biosciences, Inc)[62]

Nucleus-specific effect of MK-5046 on TBAT.

Mice (Brs3-Cre;Ai9 or WT) were transiently anesthetized with 1.5% isoflurane followed by ip urethane (1.5 g/kg; U2500, Sigma) and placed in a stereotaxic instrument. Tb was kept constant at 35 C with a homeothermic blanket system (Stoelting). TBAT was recorded with a 4600 Thermometer and a small surface temperature probe (Measurement Specialties; Fisher Scientific). 50 nl of BRS3 agonist MK-5046 (1 mg/ml in saline) or vehicle (saline) was injected (rate: 25 nl/min). After injections, all mice received 300 nl of 1g/ml PGE2 (Tocris) injections in the POA to confirm intact BAT thermogenesis. All injection sites were marked with 25 nl 0.2% Fluospheres (Life Technologies). After experiments the brains were removed, drop-fixed in 10% formalin, sectioned and mounted to verify injection sites. Mice that did not respond to PGE2 or had missed injections were excluded from analysis.

Chemogenetics.

Virus injections.—Brs-Cre mice received bilateral injections of 100 nl AAV8-hSyn-DIO-hM3Dq-mCherry in the DMH (AP: −1.85; ML: +/− 0.3; DV: −5.05, mm from bregma) or 50 nl in the PVH (AP: −0.90; ML: +/− 0.25; DV: −4.75, mm from bregma). For chemogenetic inhibition experiments we injected 150 nl AAV8-hSyn-DIO-hM4Di-mCherry bilaterally in the DMH of Brs3-Cre or Brs3-Cre;Ai6 and, as a control group, C57BL/6J mice, or in the PVH of Brs3-Cre mice.

General experimental procedure.—Mice received ip injections of 1.0 mg/kg CNO in sterile 0.9% saline, unless noted otherwise. After completion of all experiments mice were perfused and brains were collected and processed for mCherry immunohistochemistry. Mice with uni- and bilateral hits were used. Mice without hM3Dq or hM4Di expression or with expression outside of the target nuclei were excluded from analysis and served as additional controls for CNO.

hM3Dq physiology: Food intake (DMH/PVH).—Mice were fasted five hours before the onset of their dark cycle. Mice were dosed with CNO or vehicle 15 minutes prior to lights out. Food intake was measured two hours following dosing.

hM3Dq physiology: blood glucose and plasma lipids (DMH/PVH).—Blood glucose, triglycerides and glycerol were measured using tail blood samples in ad-lib fed chow mice during the first part of the light cycle after veh or CNO dosing. Serum was collected by tail bleeding. Blood glucose was measured with a Glucometer Contour (Bayer) and a serum sample was frozen until assayed for free fatty acids as per the assay kit manufacturer's manual (Pointe Scientific).

hM4Di physiology: Food intake (PVH).—Ad-lib fed mice were dosed with CNO or vehicle four hours into the light cycle and food was removed. After 15 minutes food was returned and food intake was measured two hours following return. Data is averages of three trials.

hM4Di physiology interventions(DMH): Low doses of lipopolysaccharide cause systemic inflammation and mild hyperthermia [63]. Mice were ip injected with lipopolysaccharide (50 g/kg). Cage switch-stress mediated increases in Tb [64,65]. Mice that had been living > 4d in a cage were switched with their neighbor's, 90 minutes after injection of Veh/CNO.

Body temperature telemetry experiments.

Surgical procedure and recording—Animals were anesthetized as above and E-Mitters (Starr Life Sciences) were implanted intraperitonially [66]. Two days before experiments mice were housed in temperature controlled chamber in their home cages on ER4000 energizer/receivers (Starr Life Sciences). Tb and activity were continuously measured by telemetry and 1 min means collected with VitalView software (Starr Life Sciences). Experiments were performed at 22 C, unless indicated otherwise.

Indirect calorimetry.

An Oxymax/CLAMS (Columbus Instruments) was used to measure Tb, total energy expenditure (TEE), RER (respiratory exchange ratio, O2 consumed:CO2 produced), and activity by beam break simultaneously in mice implanted with E-mitters [66]. Experiments were performed at 22 C or 30 C, as indicated. Sampling was every 13 minutes, measuring from 12 chambers.

DTA ablation experiment

At 11 weeks of age, Brs3-Cre mice were housed individually. Body weight, food intake, and body composition were measured, from which energy expenditure was calculated by mass balance (as above in Brs3-Cre mice validation). At 14 weeks, the DMHBrs3 ablation group (EYFP+DTA) was injected with Cre-dependent EYFP virus (AAV2-ef1a-DIO-EYFP) plus mCherry-Cre-dependent diphtheria toxin A virus (AAV8-ef1a-mCherry-FLEX-DTA) 62, 1:1 mix, 150 nl per side. The control group (EYFP) was only injected with the Cre-dependent EYFP virus, 1:2 dilution, 150 nl per side. At 15 weeks mice received tamoxifen treatment. At age 25 weeks mice were implanted E-Mitters (see above; Body temperature experiments), which precluded further body composition measurements. Tb experiments were performed at 27–29 weeks. From week 32 to 38 mice were housed at thermoneutrality

(30 C) and received high-fat diet (60% kcal fat, 5.24 metabolizable kcal/g; D12492, Research Diets).

EYFP neuron quantification.—After completion of the experiments brains were processed for histological analysis. Brs3-positive (i.e., EYFP positive) neurons in the DMH/DHA were counted in both groups in every third 40 m coronal section. Mice in the DTA+EYFP group with no or unilateral mCherry expression in the DMH were excluded from analysis, as were unilateral EYFP-expressing mice in the control group.

Cold exposure experiments and cage switch experiments.—Mice were housed in their home cages in a thermal chamber, two days before experiments to acclimate. At the beginning of the light cycle the thermal chamber temperature was switched from 22 C to 7 C for 6 h. In cage switch experiments, mice that had been living > 4d in a cage were switched with their neighbor's or lifted by their tail and placed back in their own as a handling control in a crossover design.

Optogenetics experiments.

Virus injections and fiber implant.—Brs-Cre or Brs3-Cre;Ai6 mice were injected with 75 nl AAV9-CAG-FLEX-ChR2-tdTomato, AAV9-ef1a-DIO-ChR2-eyfp or, as controls, AAV8-Eff1a-DIO-mCherry. Following virus injection, optical fibers (200 ?m diameter core; NA 0.22; Nufern), glued to ceramic zirconia ferrules (230 ?m bore; 1.25 OD diameter; Precision Fiber Products), were implanted unilaterally over the DMH (AP: −1.85; ML: 0.3; DV: −4.5, mm from bregma) or the RPa (AP: −6.0; ML: 0; DV: −5.5, mm from bregma). Fibers were fixed to the skull using C&B Metabond Quick Cement and dental acrylic.

Experimental procedures.—Mice were allowed to adapt to the fiber patch cord for at least three days prior to experiments and typically not handled on the day of the experiment. Fiber optic cables (200 m diameter; NA: 0.22, 1 m long; Doric Lenses; or, 0.5m long, ThorLabs) were connected to the implanted fiber optic cannulas with zirconia sleeves (Doric Lenses) and coupled to lasers via a fiber optic rotary joint (Doric Lenses). We adjusted the light power of the laser (473 nm; Laserglow or Opto Engine) such that the light power (measured with a fiber optic power meter; PM20A; ThorLabs) at the end of the fiber optic cable was ~10 mW. Using an online light transmission calculator for brain tissue (http://web.stanford.edu/group/dlab/cgi-bin/graph/chart.php), we estimated the light power at the DMH or RPa between 3 and 6 mW/mm2. This is an upper limit due to possible light loss between the fiber optic cable and the implanted optic fiber. Light pulses were controlled by a waveform generator (Arduino) programmed to deliver light pulses. In most experiments (unless otherwise indicated), stimulation was on for 1 s, followed by 3 s off, pulses were 10 ms delivered at 20 Hz. After the completion of experiments, fiber placement and ChR2 expression were assessed. Animals without ChR2 expression or incorrect placement of optic fibers were excluded from analysis.

Western blot analysis.—Mice received 1h of photostimulation and were euthanized and BAT and iWAT were dissected and stored at −80oC. Protein from BAT and iWAT was prepared using RIPA buffer, quantified (Pierce BCA Protein Assay Kit, Thermo Scientific,

Rockford, IL), separated in 4–20% SDS-PAGE gels (30 g/lane), transferred to PVDF membrane, and probed with anti-pHSL (1:1000, 4126L, Cell Signaling Technology), anti-HSL (1:1000, 4107S, Cell Signaling Technology), anti-UCP1 (1:5000, U6382, Sigma-Aldrich), or anti-?-TUBULIN (1:5000, T6074, Sigma-Aldrich). Signals were detected with SuperSignal West Pico Chemiluminescent Substrate (Thermo Scientific), images were scanned with ChemiDocTM Touch Imaging System (BIO-RAD).

Electrophysiology.

Verification of DREADD function.—Brs3-Cre mice (5–6 weeks) received injections of 150 nl AAV8-syn-DIO-hM3Dq-mCherry in PVH and DMH. Mice were used 4–6 weeks later. Brain slices were obtained and stored at approximately 30?C in a heated, oxygenated holding chamber containing aCSF (in mmol/l) 124 NaCl, 4.4 KCl, 2 CaCl2, 1.2 MgSO4, 1 NaH2PO4, 10.0 glucose, and 26.0 sodium bicarbonate before being transferred to a submerged recording chamber maintained at approximately 30?C (Warner Instruments, Hamden, CT). Recording electrodes (3–5?M?) were pulled with a Flaming-Brown Micropipette Puller (Sutter Instruments, Novato, CA) using thin-walled borosilicate glass capillaries. Current-clamp recordings monitoring shifts in resting membrane potential were obtained using electrodes filled with an intracellular recording solution containing (in mM): 135 K+-gluconate, 5 NaCl, 2 MgCl2, 10 HEPES, 0.6 EGTA, 4 Na2APT, 0.4 Na2GPT.

CRACM.—Brs3-Cre mice (5–10 weeks) received injections of 300 nl HSV-Ef1a-lsl-mCherry in the RPa (AP: −6.0; ML: 0; DV: −6.0, mm from bregma) and 100 nl of AAV1-Ef1a-ChR2-Eyfp bilaterally in the anterior POA (AP: 0.5; ML: +/− 0.4; DV: −5.25, mm from bregma). Mice were used 2 to 6 weeks later. Light evoked excitatory and inhibitory postsynaptic currents (EPSCs and IPSCs, respectively) were measured in voltage-clamp mode using electrodes filled with an intracellular recording solution containing (in mM): 135 Cs-methanesulfonate, 10 KCl, 10 HEPES, 1 MgCl2, 0.2 EGTA, 4 Mg-ATP, 0.3 GTP, 20 phosphocreatine. Lidocaine N-ethyl bromide (1 mg/ml) was included in the intracellular solution to block postsynaptic sodium currents. Neurons were held at ?55 mV to isolate glutamatergic synaptic transmission and record EPSCs, or +10 mV to isolate GABAergic synaptic transmission and record spontaneous IPSCs within individual neurons. Tetrodotoxin (TTX, 500 nM) and 4-Aminopyridine (4-AP, 100 M) were included in the bath aCSF (aCSF as above). The last cell’s IPSCs were blocked with picrotoxin (25 mM) and EPSCs with kynurenic acid (3mM).

Quantitative thermal imaging in freely moving mice

We measured the emissivity of shaved and unshaved skin from C57BL/6J mice as follows: A piece of dorsal skin was taped in tight contact with a 40 C metal surface in a black insulated vessel and equilibrated for 30 min, which achieved stable temperatures for >10 minutes. Emissivity was calculated as the skin temperature determined by the IR camera (FLIR Systems T650sc with emissivity set to 1, using ResearchIR 4 software) divided by the skin temperature measured with a digital thermometer. The emissivity was 0.97 0.02 for shaved skin and 0.88 0.01 for unshaved skin.

Shaved skin temperature in the interscapular and dorsal lumbar regions were used as measures of BAT and core body temperature, respectively, as others have done[67,68]. One day prior to study, a 2 × 2 cm midline area 2 cm above the tail and the interscapular region were shaved under isoflurane anesthesia. After housing overnight with the optical fiber attached in their home cage, mice were placed in a 20 × 20 cm cage (with bedding), 170 cm below the IR camera. Mice were allowed to acclimate for 3 h in the experimental enclosure. Mice then underwent 3 cycles of 20 min baseline, 20 min laser on, and 40 min post-stimulation, with IR images collected continuously (7.5 frames per second) during the 3 cycles. The maximum interscapular and lumbar temperatures were determined by a blinded observer every 2 minutes using ResearchIR (see **supplementary Figs. 7d and 9d** for sample stills).

Blood pressure and heart rate telemetry.

In a subset of mice with a Tb response to optogenetic stimulation of the DMH, we replaced the Emitter with an intra-arterial pressure telemetry probe. Continuous ambulatory intra-arterial blood pressure, heart rate, physical activity and subcutaneous (model HD-X10) or core (model HD-X11) temperature were measured with radio transmitters (Data Sciences International, St Paul, MN), after implantation in the carotid artery as described [69]. Data were sampled at 1000 Hz and processed using a PhysioTel RPC-1 receiver, and collected with Ponemah v6.30 (Data Sciences International). Unless noted, 1 min averages were used for analysis.

Retrograde HSV tracing.

300 nl of HSV-ef1a-lsl-EYFP or HSV-ef1a-lsl-mCherry was injected in the RPa of Brs3-Cre;Gad2-mCherry (colocalization, **Fig. 5**) or Brs3-Cre (CRACM, Fig.**7**) mice. Experiments were performed at least 2 weeks after tamoxifen treatment finished. Colocalization with mCherry in Brs3-Cre;Gad2-mCherry mice was quantified with confocal images.

Projection-specific monosynaptic rabies tracing.

Viral surgeries.—100 nl of a 1:1 mixture of AAV8-Ef1a-Flex-TVA-mCherry and AAV8-CAG-FLEX-RG was injected in the DMH (AP: −1.85; ML: +/− 0.3; DV: −5.05, mm from bregma) of Brs3-Cre mice. 4 weeks after tamoxifen treatment we injected 150 nl EnvA-G-deleted-Rabies-GFP in the RPa[70,71]. Some mice received 100 nl of EnvA-G-deleted-Rabies-GFP or EnvA-G-deleted-Rabies-ChR2-mCherry in the DMH as a control for retrograde infection of nuclei near the RPa and were not included in quantitative analysis. Two mice received 200 nl EnvA-G-deleted-Rabies-GFP in the RPa as a control for non-specific Egfp expression. Two mice (Brs3-Cre;Ai14) received AAV8-Ef1a-Flex-TVA-mCherry in the dDMH/DHA and EnvA-G-deleted-Rabies-GFP in the RPa as a control for non-RG-mediated retrograde infection upstream of starter cells.

Analysis.—Six days after Rabies virus injection, mice were euthanized. Brains were dissected and fixed in 10% formalin for 2 days, transferred to 30% sucrose overnight, sliced (50 m) on a freezing microtome (Leica), and collected in three series. For counting, one series of slices was mounted and cover slipped with hard set mounting medium containing DAPI. Slides were imaged with a VS120 slide scanner Olyvia software (v2.9, Olympus). Brain regions were defined according to Mouse Brain Atlas [72]. Neurons were counted as

starter neurons when mCherry (and/or tdTomato in Brs3-Cre;Ai14 mice) fluorescence was detected in GFP-expressing neurons.

Image capture and processing.

General procedure.—Overview images were captured using an Olympus BX61 motorized microscope with Olympus BX-UCB hardware (VS120 slide scanner) and processed using Olympus OlyVIA software (Olympus). Confocal imaging of individual nuclei for quantification of Brs3-positive neurons, pSTAT3-positive neurons and Fos-positive neurons was performed with an upright Zeiss Axio Observer Z1 microscope with a 10X objective, Zeiss 700 confocal hardware, and Zen software (2012; Zeiss). Z-stacks (9–12 ?m) of slices processed for fluorescence in situ hybridization were taken using the same confocal with a 40X objective and collapsed into a maximum intensity projection using Zen software. Images to illustrate expression of tdTomato, ChR2, DREADD, GCaMP or GFP were taken with VS120 slidescanner or Zeiss 700 confocal. Images were minimally processed to adjust brightness and contrast.

Analysis.—Overview images of every third coronal brain section were acquired using a slide-scanning microscope and used to qualitatively describe Brs3 neuron distribution in two Brs3Cre/Y;Ai14/+ mice. Neuron counting and colocalization analysis was performed using neuroanatomical landmarks [72]. Neurons were counted manually with the experimenter blinded to the experimental group. Data is represented as mean SEM

Quantification and statistics.

All data are represented as mean SEM or mean + SEM, unless otherwise indicated. No statistical methods were used to pre-determine sample sizes but our sample sizes are similar to those reported in previous publications3266. Data distribution was assumed to be normal, but this was not formally tested. All t-tests were two-sided. All n numbers refer to number of mice used for the experiment.

In experiments in which mice are handled, there is an increase in physical activity, Tb, and energy expenditure that lasts for about 1 h. Taking this into account, our standard quantification intervals for baseline were from 150 to 30 min before intervention (Pre), which was compared with 60 to 180 min after intervention (Post). These intervals avoid disturbances due to personnel in the animal room and the confounding effects of handling. Mice were tested in crossover experiments, using randomized order. Paired t-tests were used to analyze the within-mouse change from baseline effect between control and experimental interventions. Data collection and analysis were not performed blind to the conditions of the experiments.

Optogenetic experiments do not involve handling the mouse. Our standard analysis protocol is to average (within each mouse) five stimulation epochs done during a single day. This averaging minimizes the effects of spontaneous physical activity. For each mouse, data is normalized to the 20-min baseline immediately before laser on. Because of the body’s heat capacity, Tb increases are not instant, so we used 10 to 20 min from laser on as the response period. We used paired t-tests for within-mouse comparison of the effect of stimulation. For

comparison between more than 2 groups we used a one-way ANOVA with multiple comparison testing. Data collection and analysis were not performed blind to the conditions of the experiments

Supplementary Material

Refer to Web version on PubMed Central for supplementary material.

Acknowledgments

We thank Alexxai Kravitz for input throughout the project and critical reading of the manuscript, Alice Franks for assitance with animal husbandry, Yuning Huang and Yinyan Ma for assistance with surgeries and Audrey Noguchi and Danielle Springer of the NHLBI Murine Phenotyping Core for the cardiovascular telemetry implantation surgeries. Scott Sternson provided the AAV-ChR plasmid construct and Rachael Neve HSVs. MK-5046 was generously donated by Merck. Rabies virus was obtained from the GT3 Core Facility of the Salk Institute, which was funded by NIH-NCI CCSG: P30 014195 and NINDS R24 Core Grant and funding from NEI. This research was supported by the Intramural Research Program (DK075057 MLR, DK075062 MLR, DK075063 MLR, DK07002 MJK) of the National Institute of Diabetes and Digestive and Kidney Diseases, NIH.

References

References

1. Zhang L et al. Anatomical characterization of bombesin receptor subtype-3 mRNA expression in the rodent central nervous system. J Comp Neurol 521, 1020–1039, doi:10.1002/cne.23216 (2013). [PubMed: 22911445]
2. Jensen RT, Battey JF, Spindel ER & Benya RV International Union of Pharmacology. LXVIII. Mammalian bombesin receptors: nomenclature, distribution, pharmacology, signaling, and functions in normal and disease states. Pharmacol Rev 60, 1–42 (2008). [PubMed: 18055507]
3. Weber HC, Hampton LL, Jensen RT & Battey JF Structure and chromosomal localization of the mouse bombesin receptor subtype 3 gene. Gene 211, 125–131, doi:10.1016/S0378-1119(98)00050-X (1998). [PubMed: 9573346]
4. Xiao C & Reitman ML Bombesin-Like Receptor 3: Physiology of a Functional Orphan. Trends in endocrinology and metabolism: TEM 27, 603–605, doi:10.1016/j.tem.2016.03.003 (2016). [PubMed: 27055378]
5. Mo C et al. Characterization of NMB, GRP and their receptors (BRS3, NMBR and GRPR) in chickens. J Mol Endocrinol 59, 61–79, doi:10.1530/JME-17-0020 (2017). [PubMed: 28500250]
6. Zhang Y et al. Receptor-specific crosstalk between prostanoid E receptor 3 and bombesin receptor subtype 3. FASEB J 32, 3184–3192, doi:10.1096/fj.201700337RR (2018). [PubMed: 29401613]
7. Ohki-Hamazaki H et al. Mice lacking bombesin receptor subtype-3 develop metabolic defects and obesity. Nature 390, 165–169 (1997). [PubMed: 9367152]
8. Ladenheim EE et al. Factors contributing to obesity in bombesin receptor subtype-3-deficient mice. Endocrinology 149, 971–978, doi:10.1210/en.2007-1319 (2008). [PubMed: 18039774]
9. Brommage R et al. High-throughput screening of mouse knockout lines identifies true lean and obese phenotypes. Obesity 16, 2362–2367, doi:10.1038/oby.2008.361 (2008). [PubMed: 18719666]
10. Lateef DM et al. Bombesin-like receptor 3 regulates blood pressure and heart rate via a central sympathetic mechanism. Am J Physiol Heart Circ Physiol 310, H891–898, doi:10.1152/ajpheart.00963.2015 (2016). [PubMed: 26801314]
11. Lateef DM, Abreu-Vieira G, Xiao C & Reitman ML Regulation of body temperature and brown adipose tissue thermogenesis by bombesin receptor subtype-3. American journal of physiology. Endocrinology and metabolism 306, E681–687, doi:10.1152/ajpendo.00615.2013 (2014). [PubMed: 24452453]

12. Guan XM et al. Regulation of energy homeostasis by bombesin receptor subtype-3: selective receptor agonists for the treatment of obesity. Cell metabolism 11, 101–112, doi:10.1016/j.cmet.2009.12.008 (2010). [PubMed: 20096642]
13. Guan XM et al. Antiobesity effect of MK-5046, a novel bombesin receptor subtype-3 agonist. J Pharmacol Exp Ther 336, 356–364, doi:10.1124/jpet.110.174763 (2011). [PubMed: 21036912]
14. Reitman ML et al. Pharmacokinetics and pharmacodynamics of MK-5046, a bombesin receptor subtype-3 (BRS-3) agonist, in healthy patients. J Clin Pharmacol 52, 1306–1316, doi:10.1177/0091270011419854 (2012). [PubMed: 22162541]
15. Nio Y et al. A Novel Selective Bombesin Receptor Subtype 3 Agonist Promotes Weight Loss in Male Diet-Induced Obese Rats with Circadian Rhythm Change. Endocrinology, doi:10.1210/en.2016-1825 (2017).
16. Xiao C et al. Bombesin-like receptor 3 (Brs3) expression in glutamatergic, but not GABAergic, neurons is required for regulation of energy metabolism. Molecular metabolism 6, 1540–1550, doi:10.1016/j.molmet.2017.08.013 (2017). [PubMed: 29107299]
17. Liu J et al. Molecular Basis of the Pharmacological Difference between Rat and Human Bombesin Receptor Subtype-3 (BRS-3). Biochemistry 41, 8954–8960, doi:10.1021/bi0202777 (2002). [PubMed: 12102638]
18. Tan CL et al. Warm-Sensitive Neurons that Control Body Temperature. Cell 167, 47–59 e15, doi:10.1016/j.cell.2016.08.028 (2016). [PubMed: 27616062]
19. Song K et al. The TRPM2 channel is a hypothalamic heat sensor that limits fever and can drive hypothermia. Science 353, 1393–1398, doi:10.1126/science.aaf7537 (2016). [PubMed: 27562954]
20. Boulant JA Role of the Preoptic-Anterior Hypothalamus in Thermoregulation and Fever. Clinical Infectious Diseases 31, S157–S161, doi:10.1086/317521 (2000). [PubMed: 11113018]
21. Zhao ZD et al. A hypothalamic circuit that controls body temperature. Proc Natl Acad Sci U S A 114, 2042–2047, doi:10.1073/pnas.1616255114 (2017). [PubMed: 28053227]
22. Morrison SF Central neural control of thermoregulation and brown adipose tissue. Auton Neurosci 196, 14–24, doi:10.1016/j.autneu.2016.02.010 (2016). [PubMed: 26924538]
23. Nakamura K & Morrison SF Central efferent pathways for cold-defensive and febrile shivering. J Physiol 589, 3641–3658, doi:10.1113/jphysiol.2011.210047 (2011). [PubMed: 21610139]
24. Cano G et al. Anatomical substrates for the central control of sympathetic outflow to interscapular adipose tissue during cold exposure. J Comp Neurol 460, 303–326, doi:10.1002/cne.10643 (2003). [PubMed: 12692852]
25. Jeong JH et al. Cholinergic neurons in the dorsomedial hypothalamus regulate mouse brown adipose tissue metabolism. Molecular metabolism 4, 483–492, doi:10.1016/j.molmet.2015.03.006 (2015). [PubMed: 26042202]
26. Rezai-Zadeh K et al. Leptin receptor neurons in the dorsomedial hypothalamus are key regulators of energy expenditure and body weight, but not food intake. Molecular metabolism 3, 681–693, doi:10.1016/j.molmet.2014.07.008 (2014). [PubMed: 25352997]
27. Garfield AS et al. Dynamic GABAergic afferent modulation of AgRP neurons. Nat Neurosci 19, 1628–1635, doi:10.1038/nn.4392 (2016). [PubMed: 27643429]
28. Kataoka N, Hioki H, Kaneko T & Nakamura K Psychological stress activates a dorsomedial hypothalamus-medullary raphe circuit driving brown adipose tissue thermogenesis and hyperthermia. Cell metabolism 20, 346–358, doi:10.1016/j.cmet.2014.05.018 (2014). [PubMed: 24981837]
29. Cao WH & Morrison SF Glutamate receptors in the raphe pallidus mediate brown adipose tissue thermogenesis evoked by activation of dorsomedial hypothalamic neurons. Neuropharmacology 51, 426–437, doi:10.1016/j.neuropharm.2006.03.031 (2006). [PubMed: 16733059]
30. Dimicco JA & Zaretsky DV The dorsomedial hypothalamus: a new player in thermoregulation. Am J Physiol Regul Integr Comp Physiol 292, R47–63, doi:10.1152/ajpregu.00498.2006 (2007). [PubMed: 16959861]
31. Zhang Y et al. Leptin-receptor-expressing neurons in the dorsomedial hypothalamus and median preoptic area regulate sympathetic brown adipose tissue circuits. J Neurosci 31, 1873–1884, doi:10.1523/JNEUROSCI.3223-10.2011 (2011). [PubMed: 21289197]

32. Machado NLS et al. A Glutamatergic Hypothalamomedullary Circuit Mediates Thermogenesis, but Not Heat Conservation, during Stress-Induced Hyperthermia. Current Biology, doi:10.1016/j.cub.2018.05.064 (2018).
33. Allison MB et al. TRAP-seq defines markers for novel populations of hypothalamic and brainstem LepRb neurons. Molecular metabolism 4, 299–309, doi:10.1016/j.molmet.2015.01.012 (2015). [PubMed: 25830093]
34. Zeng W et al. Sympathetic neuro-adipose connections mediate leptin-driven lipolysis. Cell 163, 84–94, doi:10.1016/j.cell.2015.08.055 (2015). [PubMed: 26406372]
35. Dampney RA Central mechanisms regulating coordinated cardiovascular and respiratory function during stress and arousal. Am J Physiol Regul Integr Comp Physiol 309, R429–443, doi:10.1152/ajpregu.00051.2015 (2015). [PubMed: 26041109]
36. Viollet C et al. Somatostatin-IRES-Cre Mice: Between Knockout and Wild-Type? Frontiers in endocrinology 8, doi:10.3389/fendo.2017.00131 (2017).
37. Shah BP et al. MC4R-expressing glutamatergic neurons in the paraventricular hypothalamus regulate feeding and are synaptically connected to the parabrachial nucleus. Proc Natl Acad Sci U S A 111, 13193–13198, doi:10.1073/pnas.1407843111 (2014). [PubMed: 25157144]
38. An JJ, Liao GY, Kinney CE, Sahibzada N & Xu B Discrete BDNF Neurons in the Paraventricular Hypothalamus Control Feeding and Energy Expenditure. Cell metabolism 22, 175–188, doi:10.1016/j.cmet.2015.05.008 (2015). [PubMed: 26073495]
39. Pei H, Sutton AK, Burnett KH, Fuller PM & Olson DP AVP neurons in the paraventricular nucleus of the hypothalamus regulate feeding. Molecular metabolism 3, 209–215, doi:10.1016/j.molmet.2013.12.006 (2014). [PubMed: 24634830]
40. Sutton AK et al. Control of food intake and energy expenditure by Nos1 neurons of the paraventricular hypothalamus. J Neurosci 34, 15306–15318, doi:10.1523/JNEUROSCI.0226-14.2014 (2014). [PubMed: 25392498]
41. Cannon B & Nedergaard J Brown adipose tissue: function and physiological significance. Physiol Rev 84, 277–359, doi:10.1152/physrev.00015.2003 (2004). [PubMed: 14715917]
42. Nguyen NL et al. Separate and shared sympathetic outflow to white and brown fat coordinately regulates thermoregulation and beige adipocyte recruitment. Am J Physiol Regul Integr Comp Physiol 312, R132–R145, doi:10.1152/ajpregu.00344.2016 (2017). [PubMed: 27881398]
43. Simonds SE et al. Leptin mediates the increase in blood pressure associated with obesity. Cell 159, 1404–1416, doi:10.1016/j.cell.2014.10.058 (2014). [PubMed: 25480301]
44. Thompson RH & Swanson LW Organization of inputs to the dorsomedial nucleus of the hypothalamus: a reexamination with Fluorogold and PHAL in rat. Brain Research Reviews 27, 89–118 (1998). [PubMed: 9622601]
45. Fontes MA et al. Asymmetric sympathetic output: The dorsomedial hypothalamus as a potential link between emotional stress and cardiac arrhythmias. Auton Neurosci, doi:10.1016/j.autneu.2017.01.001 (2017).
46. Nakamura K Neural circuit for psychological stress-induced hyperthermia. Temperature (Austin) 2, 352–361, doi:10.1080/23328940.2015.1070944 (2015). [PubMed: 27227049]
47. Nakamura K & Morrison SF Central efferent pathways mediating skin cooling-evoked sympathetic thermogenesis in brown adipose tissue. American Journal of Physiology - Regulatory, Integrative and Comparative Physiology 292, R127–R136, doi:10.1152/ajpregu.00427.2006 (2007).
48. Morrison SF Central control of body temperature. F1000Res 5, doi:10.12688/f1000research.7958.1 (2016).
49. Cao WH, Fan W & Morrison SF Medullary pathways mediating specific sympathetic responses to activation of dorsomedial hypothalamus. Neuroscience 126, 229–240, doi:10.1016/j.neuroscience.2004.03.013 (2004). [PubMed: 15145088]
50. Dimitrov EL, Kim YY & Usdin TB Regulation of hypothalamic signaling by tuberoinfundibular peptide of 39 residues is critical for the response to cold: a novel peptidergic mechanism of thermoregulation. J Neurosci 31, 18166–18179, doi:10.1523/JNEUROSCI.2619-11.2011 (2011). [PubMed: 22159128]
51. Madisen L et al. A robust and high-throughput Cre reporting and characterization system for the whole mouse brain. Nat Neurosci 13, 133–140, doi:10.1038/nn.2467 (2010). [PubMed: 20023653]

52. Peron SP, Freeman J, Iyer V, Guo C & Svoboda K A Cellular Resolution Map of Barrel Cortex Activity during Tactile Behavior. Neuron 86, 783–799, doi:10.1016/j.neuron.2015.03.027 (2015). [PubMed: 25913859]
53. Szymczak-Workman AL, Vignali KM & Vignali DA Generation of 2A-linked multicistronic cassettes by recombinant PCR. Cold Spring Harb Protoc 2012, 251–254, doi:10.1101/pdb.prot067884 (2012). [PubMed: 22301657]
54. Ravussin Y, Gutman R, LeDuc CA & Leibel RL Estimating energy expenditure in mice using an energy balance technique. Int J Obes 37, 399–403 (2013).
55. Sebhat IK et al. Discovery of MK-5046, a Potent, Selective Bombesin Receptor Subtype-3 Agonist for the Treatment of Obesity. ACS Med Chem Lett 2, 43–47, doi:10.1021/ml100196d (2011). [PubMed: 24900253]
56. Graves JA Did sex chromosome turnover promote divergence of the major mammal groups?: De novo sex chromosomes and drastic rearrangements may have posed reproductive barriers between monotremes, marsupials and placental mammals. Bioessays 38, 734–743, doi:10.1002/bies.201600019 (2016). [PubMed: 27334831]
57. Qi J et al. VTA glutamatergic inputs to nucleus accumbens drive aversion by acting on GABAergic interneurons. Nat Neurosci 19, 725–733, doi:10.1038/nn.4281 (2016). [PubMed: 27019014]
58. Stratigopoulos G et al. Hypomorphism of Fto and Rpgrip1l causes obesity in mice. J Clin Invest 126, 1897–1910, doi:10.1172/JCI85526 (2016). [PubMed: 27064284]
59. Fox DA et al. Gestational lead exposure selectively decreases retinal dopamine amacrine cells and dopamine content in adult mice. Toxicol Appl Pharmacol 256, 258–267, doi:10.1016/j.taap.2011.05.021 (2011). [PubMed: 21703292]
60. Geerling JC, Yokota S, Rukhadze I, Roe D & Chamberlin NL Kolliker-Fuse GABAergic and glutamatergic neurons project to distinct targets. J Comp Neurol 525, 1844–1860, doi:10.1002/cne.24164 (2017). [PubMed: 28032634]
61. Wu Z, Autry AE, Bergan JF, Watabe-Uchida M & Dulac CG Galanin neurons in the medial preoptic area govern parental behaviour. Nature 509, 325–330, doi:10.1038/nature13307 (2014). [PubMed: 24828191]
62. Saunders A, Johnson CA & Sabatini BL Novel recombinant adeno-associated viruses for Cre activated and inactivated transgene expression in neurons. Front Neural Circuits 6, 47, doi:10.3389/fncir.2012.00047 (2012). [PubMed: 22866029]
63. Rudaya AY, Steiner AA, Robbins JR, Dragic AS & Romanovsky AA Thermoregulatory responses to lipopolysaccharide in the mouse: dependence on the dose and ambient temperature. Am J Physiol Regul Integr Comp Physiol 289, R1244–1252, doi:10.1152/ajpregu.00370.2005 (2005). [PubMed: 16081879]
64. Lee DL, Webb RC & Brands MW Sympathetic and angiotensin-dependent hypertension during cage-switch stress in mice. Am J Physiol Regul Integr Comp Physiol 287, R1394–1398, doi:10.1152/ajpregu.00306.2004 (2004). [PubMed: 15308486]
65. Lateef DM, Abreu-Vieira G, Xiao C & Reitman ML Regulation of body temperature and brown adipose tissue thermogenesis by bombesin receptor subtype-3. American journal of physiology. Endocrinology and metabolism 306, E681–687, doi:10.1152/ajpendo.00615.2013 (2014). [PubMed: 24452453]
66. Lute B et al. Biphasic effect of melanocortin agonists on metabolic rate and body temperature. Cell metabolism 20, 333–345, doi:10.1016/j.cmet.2014.05.021 (2014). [PubMed: 24981835]
67. Vianna DML & Carrive P Stress-induced hyperthermia is not mediated by brown adipose tissue in mice. Journal of Thermal Biology 37, 125–129, doi:10.1016/j.jtherbio.2011.11.010 (2012).
68. Gachkar S et al. 3-Iodothyronamine Induces Tail Vasodilation Through Central Action in Male Mice. Endocrinology 158, 1977–1984, doi:10.1210/en.2016-1951 (2017). [PubMed: 28368510]
69. Kim SM et al. Salt sensitivity of blood pressure in NKCC1-deficient mice. Am J Physiol Renal Physiol 295, F1230–1238, doi:10.1152/ajprenal.90392.2008 (2008). [PubMed: 18701622]
70. Stornetta RL, Inglis MA, Viar KE & Guyenet PG Afferent and efferent connections of C1 cells with spinal cord or hypothalamic projections in mice. Brain Struct Funct 221, 4027–4044, doi:10.1007/s00429-015-1143-3 (2016). [PubMed: 26560463]

71. Betley JN, Cao ZF, Ritola KD & Sternson SM Parallel, redundant circuit organization for homeostatic control of feeding behavior. Cell 155, 1337–1350, doi:10.1016/j.cell.2013.11.002 (2013). [PubMed: 24315102]

72. Paxinos G & Franklin KBJ The mouse brain in stereotaxic coordinates. Compact 3rd edn, (Elsevier Academic Press, 2008).

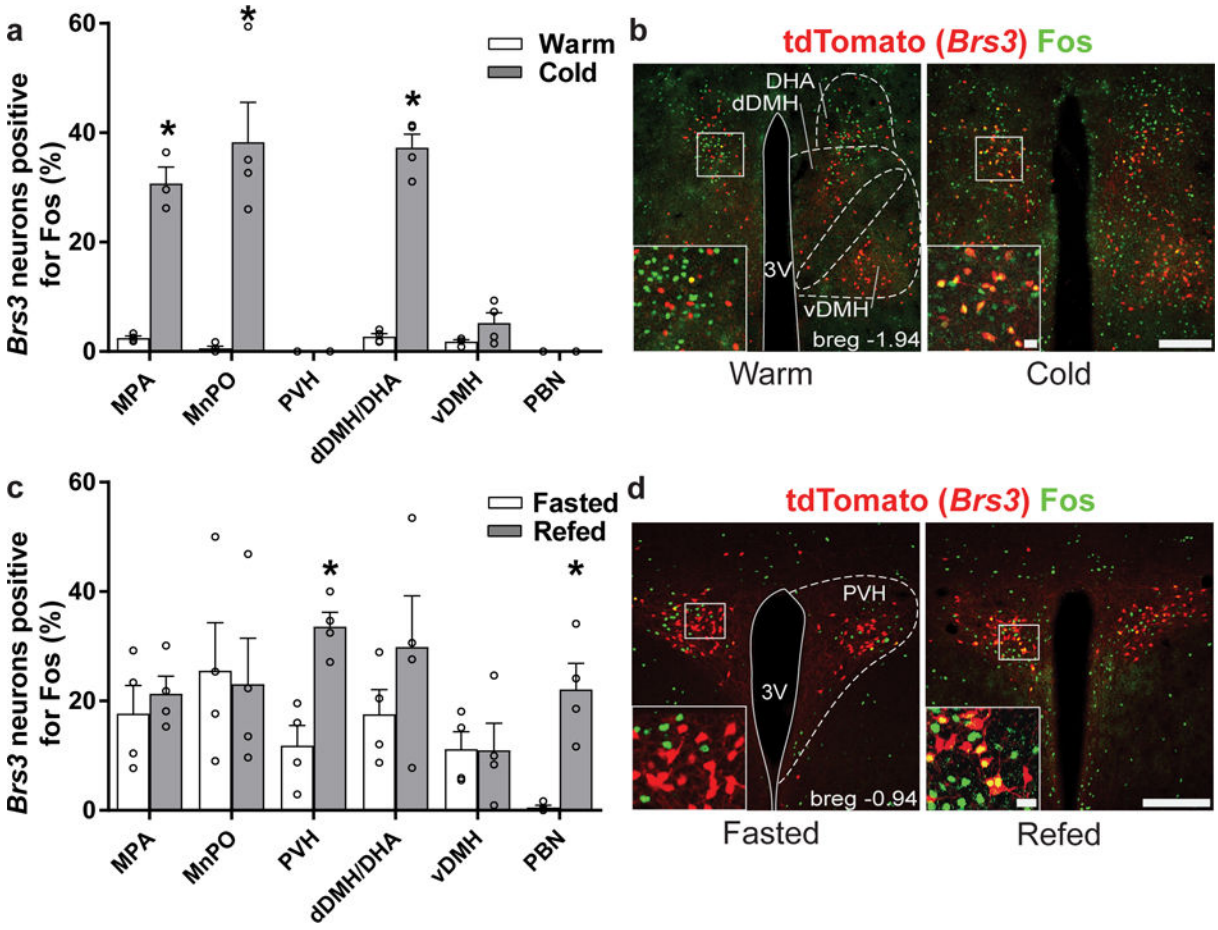

Figure 1. *Brs3* neurons are differentially activated by exposure to a cold environment and by refeeding.

(a) Percentage of *Brs3* neurons positive for Fos following cold (4 °C) or warm (30 °C) exposure. The environmental temperature did not affect total number of *Brs3*-positive neurons (100% is 171 ± 15 in the MPA, 125 ± 12 in the MnPO, 181 ± 15 in the PVH, 134 ± 10 in the dDMH/DHA, 255 ± 26 in the vDMH, and 214 ± 18 in the PBN; mean ± SEM). * indicates $p<0.05$ by unpaired two-sided t-test within region: MPA, $p = 0.0001$; MnPO, $p = 0.002$; dDMH/DHA, $p = 0.0005$. (b) Examples of DMH/DHA sections from Brs3-Cre;Ai14 mice stained for Fos after warm or cold exposure. (c) Percentage of *Brs3* neurons positive for Fos following a 20h fast or fast and 2h of refeeding. The total number of *Brs3*-positive neurons was not affected by fasting or refeeding (100% is 166 ± 20 in the MPA, 99 ± 17 in the MnPO, 190 ± 9 in the PVH, 137 ± 12 in the dDMH/DHA, 232 ± 25 in the vDMH and 225 ± 18 in the PBN). * indicates $p<0.05$ by unpaired two-sided t-test within region: PVH, $p = 0.003$; PBN, $p = 0.004$. (d) Examples of Brs3-Cre;Ai14 PVH sections stained for Fos after fasting or refeeding. a,c. n = 4/group, with 2–3 sections per mouse. Data are mean + SEM. Scale bar in b,d 200 μm; 20 μm in inset.

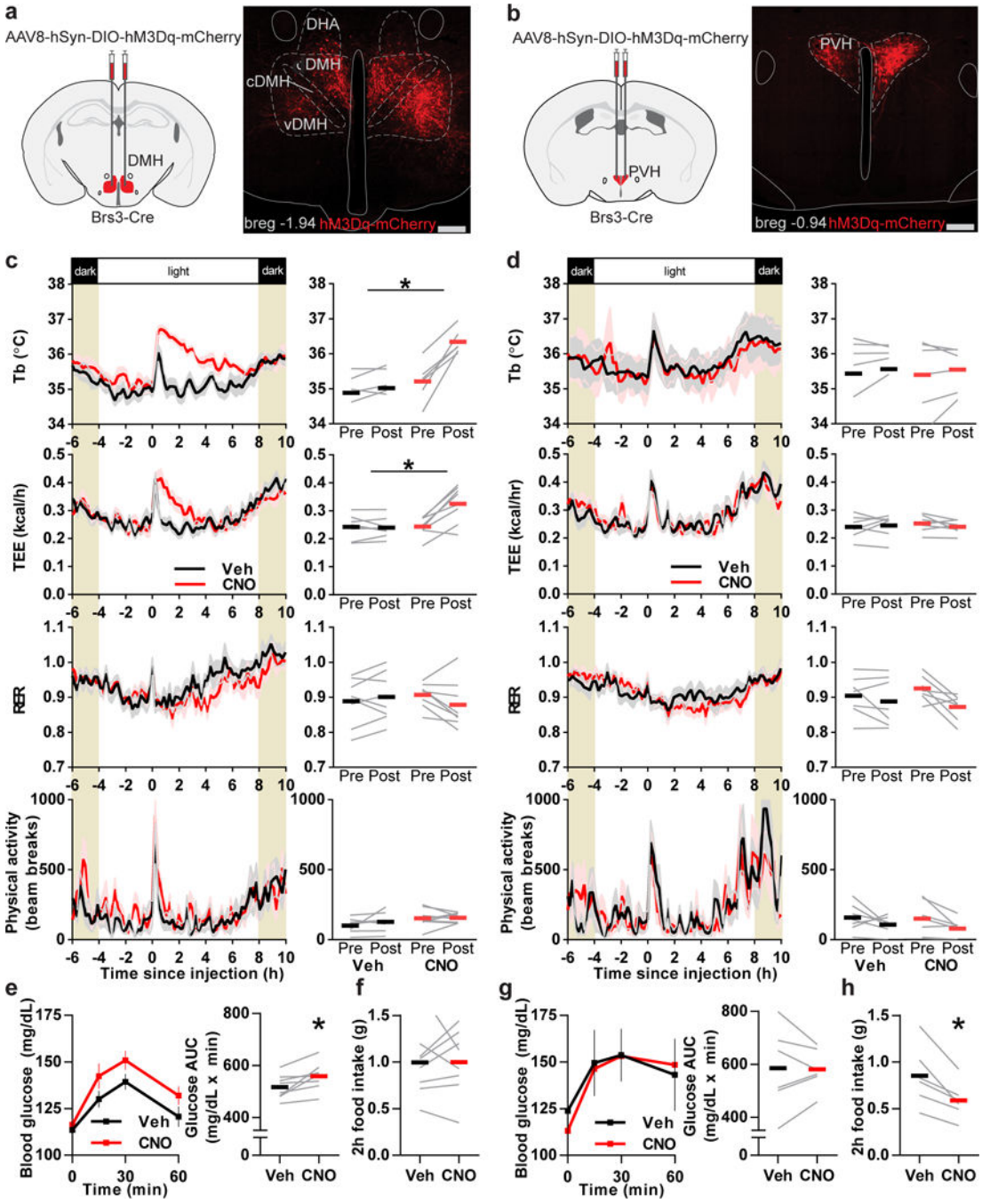

Figure 2. Activation of DMH^{Brs3} neurons increases Tb and activation of PVH^{Brs3} neurons suppresses food intake.

(a, b) Schematic of virus injection (left) and representative expression of hM3Dq-mCherry (right) in DMH (a) and PVH (b). Scale bar, 200 μm. (c, d) Tb, total energy expenditure (TEE), respiratory exchange ratio (RER: vCO_2/vO_2) and physical activity response to CNO (1 mg/kg) or vehicle in DMH^{Brs3}::hM3Dq (c, n = 8) and PVH^{Brs3}::hM3Dq (d, n = 7) mice at 30°C. For quantification, Pre is mean from −150 to −30 and Post from 60 to 180 min. * p values, paired two-sided t-test on change from baseline, CNO vs vehicle: DMH Tb, p = 0.003; DMH TEE, p = 0.005. (e, g) Blood glucose response to CNO (1 mg/kg) in ad lib fed

DMH^{Brs3}::hM3Dq (e; n = 8/group) and PVH^{Brs3}::hM3Dq (g; n = 6/group) mice during light cycle. * indicates p = 0.02 by paired two-sided t-test, CNO vs vehicle. (f, h) Effect of CNO (1 mg/kg) on food intake (using average of two trials/mouse) at onset of dark cycle after 5 h fast in DMH^{Brs3}::hM3Dq (f; n = 8/group) and PVH^{Brs}3::hM3Dq (h; n = 6/group) mice. * indicates p = 0.008 by paired two-sided t-test, CNO vs vehicle. (c-h) Crossover design. Data are mean ± SEM in left panels of (c-e, g). Black (vehicle) and red (CNO) bars represent means.

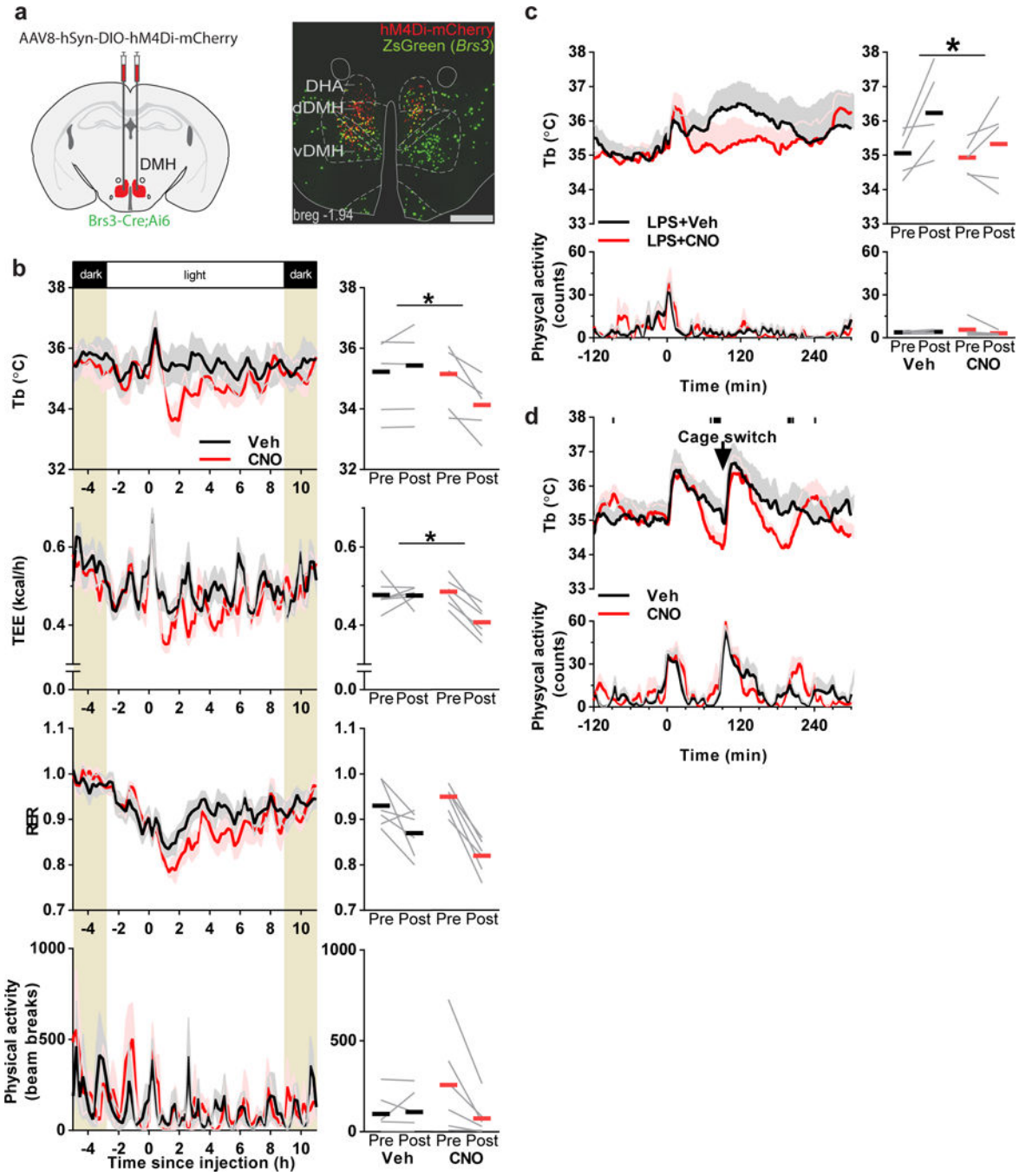

Figure 3. Inhibition of DMH^{Brs3} neurons reduces TEE and Tb.

(a) Schematic of virus injection (left) and representative example of hM4Di-mCherry expression in DMH of Brs3-Cre;Ai6 mice (right). Scale bar, 500 μm. (b) Tb, TEE, RER (vCO_2/vO_2), and physical activity response to CNO (1 mg/kg) or vehicle in DMH^{Brs3}::hM4Di mice at 22 °C (n = 6/group). Data are mean ± SEM, crossover design. * p values, paired two-sided t-test of the change from baseline, CNO vs vehicle: Tb, p = 0.02; TEE, p = 0.03. (c) Effect of CNO (1 mg/kg) in DMH^{Brs3}::hM4Di mice on response to lipopolysaccharide (LPS) treatment (50 μg/kg, ip). (d) Effect of CNO (1 mg/kg) in

DMH^{Brs3}::hM4Di mice in response to cage switch, (n = 5 /group). Black rectangles at the top of the graph indicate $p<0.05$ by paired two-sided t-test, CNO vs vehicle, for individual data points, without multiplicity correction. (b,c) For quantification, Pre is mean from −150 to −30 and Post is 60 to 180 min. Black (vehicle) and red (CNO) bars represent means. (c,d) Data are mean + SEM, crossover design.

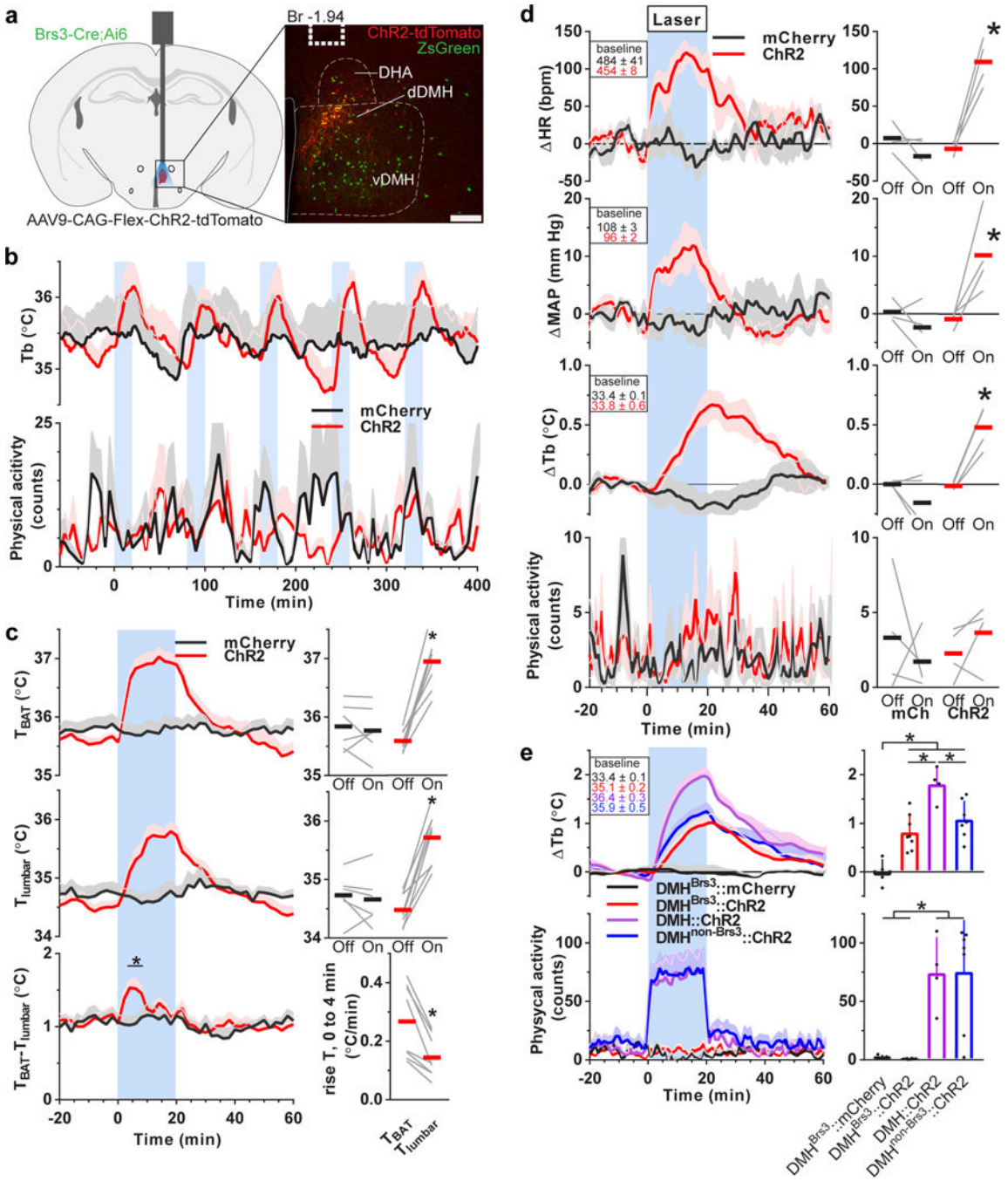

Figure 4. Optogenetic activation of DMH^{Brs3} neurons increases Tb, T_{BAT}, HR and MAP, but not physical activity.

(a) Schematic of laser stimulation (left) and representative expression of ChR2 and optic fiber placement (dotted line) in DMH (right). Scale bar represents 200 μm. (b) Tb and physical activity during repeated cycles with 20 min epochs of optogenetic stimulation (blue interval) of DMH^{Brs3}::ChR2 (n = 8) and DMH^{Brs3}::mCherry (n = 6) mice. Data are mean + SEM. (c) Infrared camera interscapular (T_{BAT}, top left) and lumbar (T_{lumbar}, middle left) skin temperature measurements during optogenetic stimulation (blue interval) of DMH^{Brs3}::ChR2 (n = 8) and DMH^{Brs3}::mCherry (n = 7) mice. Data are mean + SEM. For

quantification of T_{BAT} (top right) and T_{lumbar} (middle right), Off is −10 to −2 and On is 10 to 18 min. * p = 0.0001, paired two-sided t-test. Bottom left panel, difference between T_{BAT} and T_{lumbar}. * p<0.03 at t = 4,6,8 min, unpaired two-sided t-test, DMH^{Brs3}::ChR2 vs DMH^{Brs3}::mCherry. Bottom right panel: initial rate of increase in T_{BAT} and T_{lumbar} in DMH^{Brs3}::ChR2 mice (from 0 to 4 min of laser on). * p = 0.002, paired two-sided t-test. (d) Heart rate (HR), mean arterial pressure (MAP), Tb and physical activity responses to laser (blue interval) in DMH^{Brs3}::ChR2 and DMH^{Brs3}::mCherry mice (n = 4/group) in left panels (data are mean ± SEM). Temperature data from subcutaneously and intraperitoneally implanted DSI transmitters were pooled and represented as Tb. Data (mean of 5 epochs) is normalized to −20 to 0 min (baseline). For quantification in right panels, Off is −10 to 0 and On is 11 to 20 min. * p values, paired two-sided t-test, Off vs On: ΔHR, p = 0.006; ΔMAP, p = 0.047; ΔTb, p = 0.007. (e) Summary of Tb and physical activity in DMH^{Brs3}::mCherry (black), DMH^{Brs3}::ChR2 (red), DMH::ChR2 (violet), and $DMH^{non\text{-}Brs3}$::ChR2 (blue) mice. Data are means + SEM of data from **Fig. 4b** and **Supplementary Fig. 9b**. For quantification, the mean difference is between −10 to 0 and 11 to 20 min is used. * p<0.05 one-way ANOVA, with Tukey's multiple comparison test. Laser stimulation (blue intervals) was alternating 1 s on (20 Hz, 10 ms pulses) with 3 s off for 20 min. (c, d) Bars are means (red: mCherry; black: ChR2).

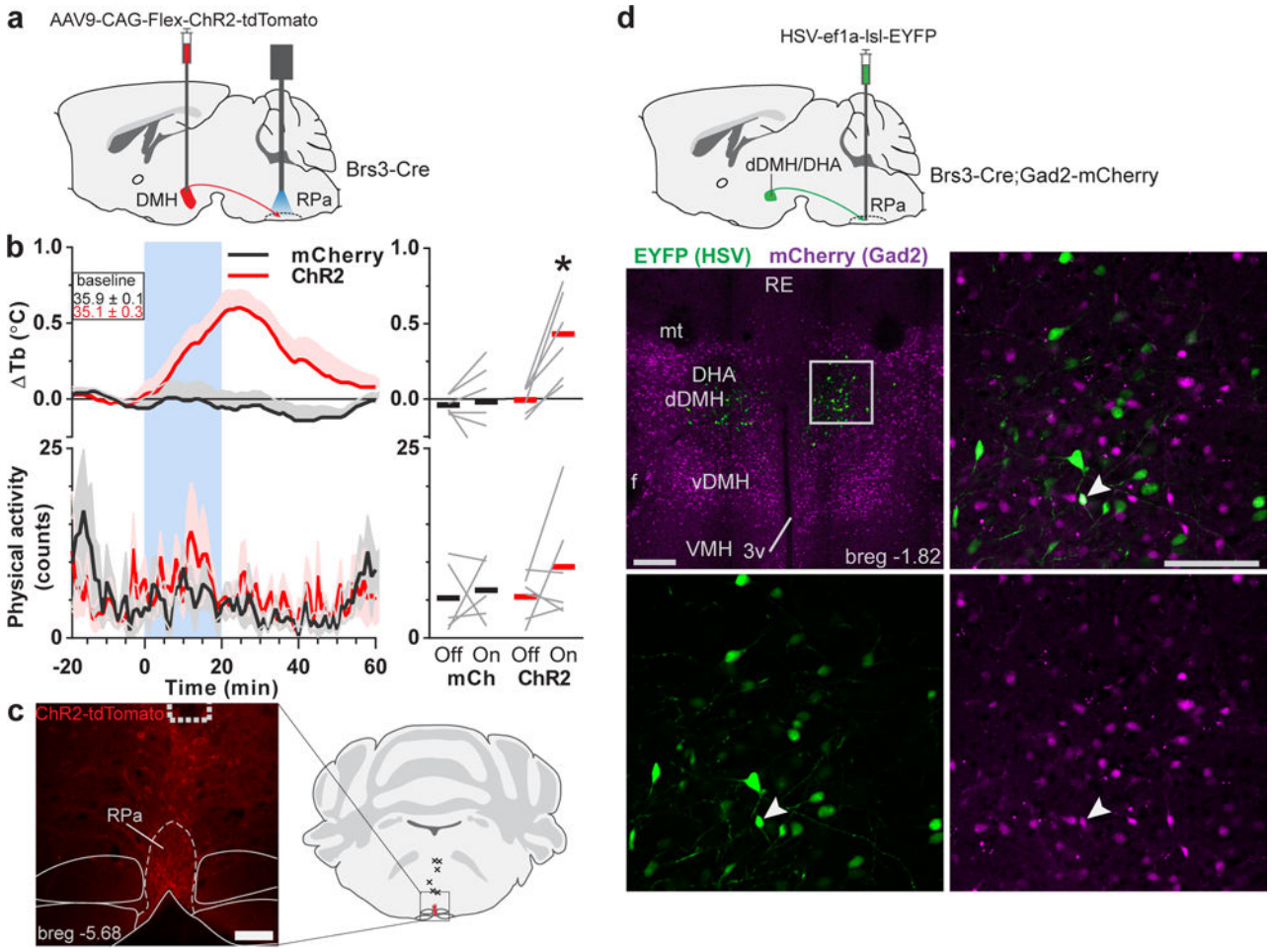

Figure 5. Optogenetic stimulation of DMH^{Brs3} →RPa terminals increases Tb, possibly via glutamate.

(a) Schematic of virus (AAV-Flex-ChR2) injection in the DMH and laser stimulation of the RPa. (b) Tb response to optogenetic stimulation (blue interval) of DMH^{Brs3}→RPa terminals in DMH^{Brs3}::ChR2 (n = 6) and control DMH^{Brs3}::mCherry (n = 6) mice. Data are change from −20 to 0 min and are mean + SEM (left). For quantification, Off is mean from −10 to 0 and On from 11 to 20 min. * p = 0.006, paired two-sided t-test, Off vs On. Black (mCherry) and red (ChR2) bars represent means. (c) Representative section showing DMH^{Brs3}→RPa terminals (left; fiber indicated by dotted lines) and schematic of fiber placement (right, fiber positions indicated by x). Scale bar represents 100 μm. (d) Schematic of retrograde Cre-dependent EYFP-expressing HSV injected into the RPa of Brs3-Cre;Gad2-mCherry mice. EYFP-positive neurons are DMH^{Brs3}→RPa. mCherry-positive neurons express Gad2. Arrowhead indicates colocalization. We counted 72 ± 13 EYFP neurons per animal (4 mice, two slices per mouse). Scale bar overview, 250 μm, inset 100 μm. Abbreviations: DHA - dorsal hypothalamic area; d/vDMH - dorsal/ventral dorsomedial hypothalamus; f - fornix; mt - mammillothalamic tract; RE - nucleus of reuniens; VMH - ventromedial hypothalamus; 3v - 3rd ventricle

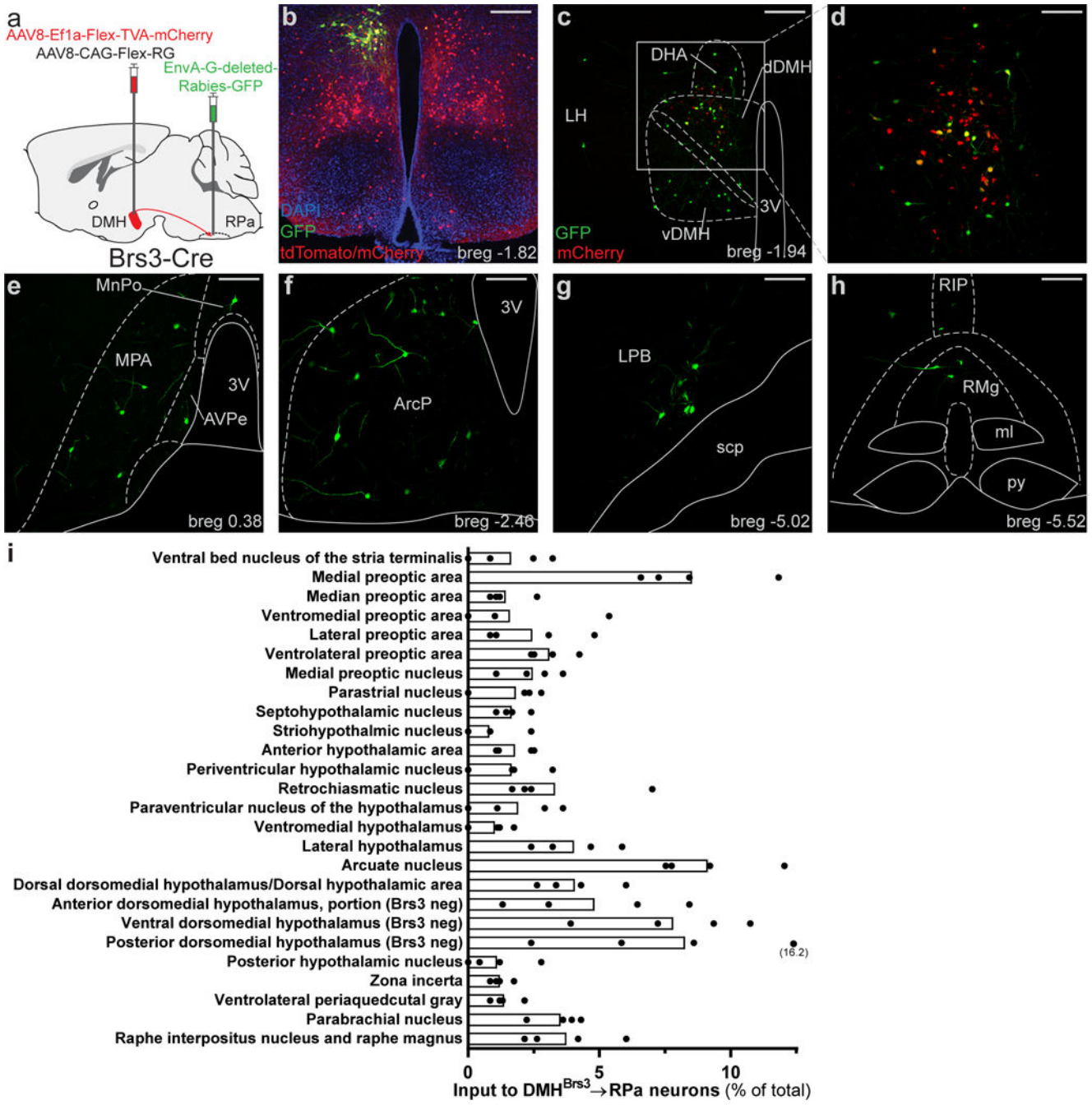

Figure 6. DMH^{Brs3}→RPa neurons receive input from POA and other nuclei.

(a) Schematic of projection-specific rabies tracing. (b) Brs3-Cre;Ai14 mice injected with AAV-DIO-TVA-mCherry in the DMH and EnvA-G-deleted-Rabies-GFP in the RPa, showing the dDMH/DHA localization of DMH^{Brs3}→RPa neurons. (c-i) Brs3-Cre mice were injected with Flex-TVA-mCherry and Flex-RG viruses in the DMH and EnvA-G-deleted-Rabies-GFP in the RPa. (c,d) DMH showing DMHBrs3→RPa starter neurons expressing TVA-mCherry and GFP. (d) higher magnification of inset. (e-h) Examples of regions with higher numbers of input neurons, which express only GFP. (i) Areas with input neurons to DMHBrs3→RPa neurons, percentage of total. Only areas with input neurons in at least 3 of

the 4 mice are shown. Scale bar, b,c,h 200 μm, d-g 100 μm. Abbreviations: 3V – third ventricle; ARCp – arcuate nucleus, posterior part; AVPe – periventricular nucleus, anterior ventral part; DHA – dorsal hypothalamic area; LH – lateral hypothalamus; ml – medial lemniscus; MnPO – median preoptic area; MPA – medial preoptic area; py – pyramidal tract; RIP – raphe interpositus nucleus; RMg – raphe magnus; v/dDMH – dorsomedial hypothalamus (ventral/dorsal); scp – superior cerebellar peduncle.

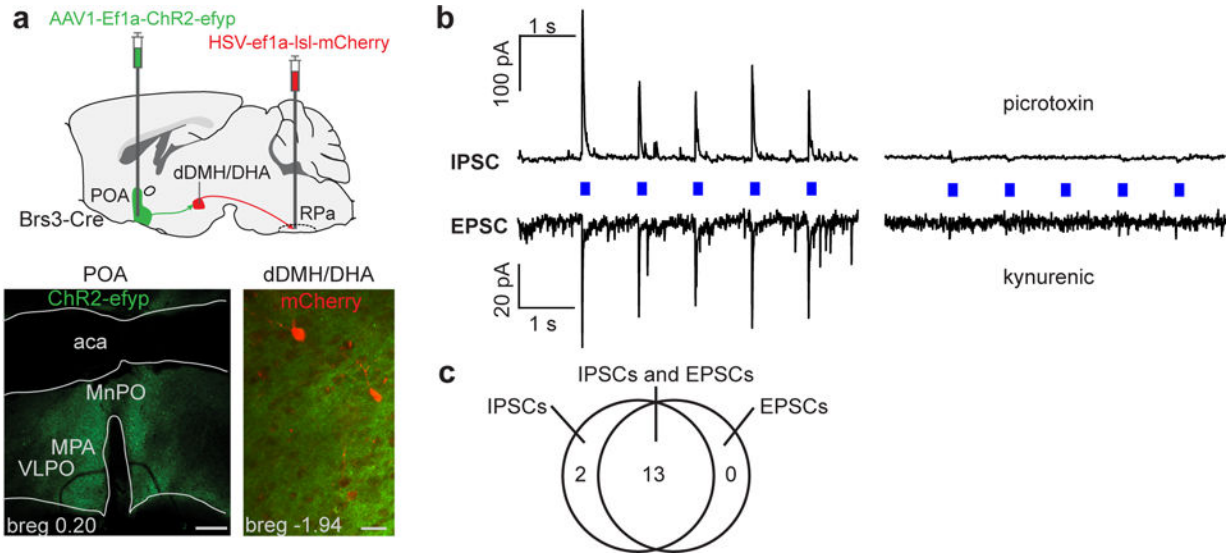

Figure 7. DMH^{Brs3}→RPa neurons receive inhibitory and excitatory input from the POA.

(a) Schematic showing injection of 1) Cre-dependent mCherry-expressing HSV in the RPa (marking DMH^{Brs3}→RPa neurons) and 2) Cre-independent ChR2-EYFP-expressing AAV in the POA. Scale bar represents 200 μm (left image) and 25 μm (right image). (b) Voltage-clamp trace of a DMH^{Brs3}→RPa neuron in a DMH-containing brain slice. Recording was made in the presence of TTX (500 nM) and 4-AP (100 μM), showing monosynaptic inhibitory and excitatory input from the POA. Picrotoxin (25 mM) and kynurenic acid (3 mM) blocked inhibitory postsynaptic currents (IPSCs) and excitatory postsynaptic currents (EPSCs), respectively. All 15 DMH^{Brs3}→RPa neurons recorded from (2 mice) had PSCs in response to light. IPSCs recorded at +10mV and EPSCs at −55mV. (c) Venn diagram of POA input to DMH^{Brs3}→RPa neurons, showing the number of each type of PSC.